

Impact of groundwater representation on heat events in regional climate simulations over Europe

Liubov Poshyvailo-Strube^{1,2}, Niklas Wagner^{1,2}, Klaus Goergen^{1,2}, Carina Furusho-Percot³, Carl Hartick^{1,2,4}, and Stefan Kollet^{1,2}

¹Institute of Bio- and Geosciences: Agrosphere (IBG-3), Forschungszentrum Jülich GmbH, Jülich, Germany

²Centre for High-Performance Scientific Computing in Terrestrial Systems (HPSC TerrSys), Geoverbund ABC/J, Jülich, Germany

³National Research Institute for Agriculture, Food and Environment (INRAE), Avignon, France

⁴Jülich Supercomputing Centre (JSC), Forschungszentrum Jülich GmbH, Jülich, Germany

Correspondence: Liubov Poshyvailo-Strube (l.poshyvailo@fz-juelich.de)

Abstract. The representation of groundwater is simplified in most regional climate models (RCMs), potentially leading to biases in the simulations. This study introduces a unique dataset from the regional Terrestrial Systems Modelling Platform (TSMP) forced by the Max Planck Institute Earth System Model at Low Resolution (MPI-ESM-LR) boundary conditions in the context of dynamical downscaling of global climate models (GCMs) for climate change studies. TSMP explicitly simulates a full 3D soil- and groundwater dynamics together with overland flow, including the complete water and energy cycles from the bedrock to the top of the atmosphere. By comparing the statistics of heat events, i.e. a series of consecutive days with a near-surface temperature exceeding the 90th percentile of the reference period, from TSMP and those from GCM-RCM simulations with simplified groundwater dynamics from the COordinated Regional Climate Downscaling EXperiment (CORDEX) for the European domain, we aim to improve the understanding of how groundwater representation affect heat events in Europe.

The analysis is carried out for the summer seasons of the period 1976-2005 relative to 1961-1990 in each RCM. While our results show that TSMP simulates heat events consistently with the CORDEX ensemble, there are some systematic differences that we attribute to the more realistic representation of groundwater in TSMP. Compared to the CORDEX ensemble, TSMP simulates fewer hot days (i.e., days with a near-surface temperature exceeding the 90th percentile of the reference period), as well as lower interannual variability and decadal change in the number hot days on average over Europe. TSMP systematically simulates fewer heat waves (i.e., heat events lasting 6 days or more) compared to the CORDEX ensemble, moreover, they are shorter and less intense. The Iberian Peninsula is particularly sensitive to the representation of groundwater. Therefore, incorporating an explicit 3D groundwater representation in RCMs may be a key in reducing biases in simulated duration, intensity, and frequency of heat events in Europe. The results highlight the importance of hydrological processes for the long-term regional climate simulations and provide indications of possible potential implications for climate change projections.

20 1 Introduction

Over the past decades, the number of heat waves has increased (e.g., Frich et al., 2002; Christidis et al., 2015; Zhang et al., 2020). The years 2003, 2010, 2018, and 2022 were among the hottest in Europe, characterised by record-breaking near-surface air temperatures (e.g., Stott et al., 2004; Barriopedro et al., 2011; Dirmeyer et al., 2021; Yule et al., 2023). With projected climate change, the occurrence of heat waves will continue to increase (e.g., Russo et al., 2015; Hari et al., 2020; Molina et al., 25 2020; Masson-Delmotte et al., 2021), leading to multiple negative socio-economic impacts (e.g., Amengual et al., 2014; Yin et al., 2022).

The physical mechanisms underlying heat waves have been extensively studied (e.g., Horton et al., 2016; Liu et al., 2020; Barriopedro et al., 2023). Heat waves are triggered by strong, persistent, quasi-stationary large-scale high pressure systems associated with atmospheric blocking events, resulting in subsiding adiabatically warmed air masses and clear skies allowing 30 for high insolation (Tomczyk and Bednorz, 2016; Kautz et al., 2022). The evolution of heat waves depends primarily on the synoptic weather patterns in combination with ambient soil moisture conditions, further altered by multiple land-atmosphere feedback processes (e.g., Fischer et al., 2007).

European summer heat waves are often preceded by a precipitation deficit in spring (e.g., Stegehuis et al., 2021; Hartick et al., 2021). Due to the long-term soil moisture memory effect, the lack of precipitation in early spring causes negative soil 35 moisture anomalies in early summer and strengthens the land-atmosphere coupling (a measure of the response of the atmosphere to anomalies in the land surface state) with a lower evaporation fraction. In turn, this reduces latent cooling and amplifies summer temperatures. Note that the soil moisture memory is a phenomenon of persistence of wet or dry anomalies over a long period of time, from weeks to months, after the atmospheric conditions that caused them have passed; this allows to preserve the hydroclimatic conditions of the preceding months (e.g., Song et al., 2019). Thus, the long-term soil moisture memory can 40 contribute to either buffering negative droughts impacts and weakening a heat wave, or, conversely, delaying drought recovery and exacerbating the occurrence of a heat wave (Erdenebat and Tomonori, 2018; Martínez-de la Torre and Miguez-Macho, 2019; Hartick et al., 2021; Dirmeyer et al., 2021). In addition to precipitation, soil moisture is strongly influenced by ground-water dynamics via vertical fluxes across the water table (capillary rise) and via horizontal fluxes through gravity-driven lateral transport within the saturated zone. Here, the water table depth dictates the intensity of shallow groundwater–soil moisture and 45 evaporation coupling (Kollet and Maxwell, 2008).

In the context of climate impact assessments, dynamical downscaling of global climate models (GCMs) with regional climate models (RCMs) is widely used to generate regional climate change scenario information (e.g., Mearns et al., 2015; Jacob et al., 2020). RCMs have been shown to provide added value to driving GCMs by better capturing small-scale processes (Giorgi and Gutowski, 2015; Torma et al., 2015; Prein et al., 2016; Rummukainen, 2016; Iles et al., 2020), but model biases (offset 50 during the historical period against observations) and uncertainties in climate projections still remain (Hawkins and Sutton, 2009; Sørland et al., 2018; Evin et al., 2021). In fact, many RCMs tend to overestimate duration, intensity and frequency of heat waves (e.g., Vautard et al., 2013; Plavcová and Kyselý, 2016; Lhotka et al., 2018; Furusho-Percot et al., 2022).

The role of soil moisture in modelling heat waves is crucial (Seneviratne et al., 2006, 2010; Fischer et al., 2007), but due to the complexity of the processes involved and related high computational cost, the explicit representation of hydrological processes is oversimplified in most RCMs. Commonly applied hydrology schemes are based on 1D-parameterizations in the vertical direction with runoff generation at the land surface and a gravity driven free drainage approach as the lower boundary condition. In such a parametrisation there is no lateral subsurface flow and only the 1D-Richards' equation is solved (e.g., Niu et al., 2007). RCMs with a simplified representation of hydrological processes have difficulties in reliably reproducing the land surface energy flux partitioning, and, consequently, near-surface air temperatures, leading to warm biases (e.g., Barlage et al., 2021). Hydrological parameters tuning (e.g., Teuling et al., 2009; Bellprat et al., 2016) or developing new parameterizations of groundwater dynamics (e.g., Liang et al., 2003; Schlemmer et al., 2018) have been shown to improve model results. Feedback mechanisms between groundwater, land surface, and atmosphere are also often simplified in RCMs. A physically consistent description of hydrological processes in RCMs can be achieved by an explicit representation of 3D soil- and groundwater hydrodynamics together with overland flow, accounting for the feedback loops over the terrestrial system and closing water and energy cycles from groundwater across the land surface to the top of the atmosphere (Maxwell et al., 2007), as for instance in the Terrestrial Systems Modelling Platform (TSMP) (e.g., Shrestha et al., 2014; Gasper et al., 2014), a regional climate system model.

Keune et al. (2016) demonstrates a relationship between the representation of groundwater dynamics and near-surface air temperature for the August 2003 European heat wave from TSMP simulations nested within the ERA-Interim reanalysis (Dee et al., 2011). In their study, the TSMP model was set up over the European domain of the COordinated Regional Climate Down-scaling EXperiment (CORDEX) (e.g., Gutowski et al., 2016; Jacob et al., 2020) with two different groundwater configurations: (i) simplified 1D free drainage approach and (ii) 3D physics-based variably saturated groundwater dynamics. The clear impact of groundwater dynamics on the land surface water and energy balance is shown: latent heat fluxes are higher and maximum temperatures are lower, especially in areas with shallow water table depth, in the 3D configuration compared to the simplified 1D free drainage approach. The work of Keune et al. (2016) suggests that 3D groundwater dynamics in TSMP alleviate the evolution of a single heat wave due to weaker land-atmosphere feedbacks compared to simplified 1D free drainage approach, at least during the investigated European heat wave of summer 2003. The ability of an explicit representation of groundwater dynamics to moderate air temperatures during a single seasonal heat wave in RCM simulations was also demonstrated in Barlage et al. (2015, 2021); Mu et al. (2022).

Further studies were carried out to understand whether the aforementioned effects of the groundwater representation persist over longer time periods in RCM evaluation runs, and how this manifests itself for heat waves over Europe. Furusho-Percot et al. (2019) shows that TSMP simulation forced by the ERA-Interim reanalysis captures climate system dynamics and the succession of warm and cold seasons at the regional scale for PRUDENCE regions (Christensen and Christensen, 2007) consistent with the E-OBS observations (Cornes et al., 2018), for the investigated period of 1996–2018. Moreover, TSMP multiannual evaluation run exhibits lower deviations of summer heat wave indices from the E-OBS observations, compared to the CORDEX RCMs with a simplified representation of groundwater, which tend to simulate too persistent heat waves (Furusho-Percot et al., 2022). This particular behaviour of TSMP is attributed to its improved hydrology, which leads to a better capacity to sustain

soil moisture and, therefore, a more reliable latent heat flux and evaporation. This leads to a decrease in the number of days with anomalously high near-surface temperatures, as well as the intensity and spatial extent of heat waves. An important question still remains: how will these findings be reflected in the long-term regional climate simulations in the context of dynamical downscaling of GCMs by RCMs for climate change studies over Europe?

In this paper, we present a unique dataset from the TSMP regional climate system model forced by the Max Planck Institute Earth System Model at Low Resolution (MPI-ESM-LR) historical boundary conditions (Giorgetta et al., 2013), over the CORDEX European domain. We interrogate the statistics of the characteristics of heat events (duration, intensity, frequency) for the summer seasons of 1976-2005 with respect to the reference period 1961-1990 in each RCM, by comparing TSMP results and the CORDEX RCMs with a simplified representation of groundwater driven by GCMs control simulations of phase five of the Coupled Model Intercomparison Project, CMIP5 (Taylor et al., 2012). We strive to better understand the impact of 3D groundwater dynamics on simulated heat events in historical regional climate simulations and potential consequences for climate change projections. While Furusho-Percot et al. (2022) examined the statistics of heat events in the TSMP evaluation run, the long-term TSMP historical climate simulations forced by MPI-ESM-LR GCM have not been previously presented or analysed. Thus, this is the first assessment of the heat event statistics over Europe from a dynamically downscaled GCM with a fully coupled RCM that comprises an explicit representation of groundwater dynamics and two-way non-linear feedbacks from groundwater across the land surface to the top of the atmosphere.

Section 2 introduces the methods, describing the TSMP modelling platform and its setup, the procedure for detection and analysis of heat events, and the CORDEX ensemble used for comparison with the TSMP results. In Sect. 3, we examine the TSMP dataset forced by MPI-ESM-LR GCM for consistency with the CORDEX ensemble and present results on the impact of an explicit groundwater representation on simulated heat events in long-term regional historical climate simulations. Section 4 contains the discussion, and Sect. 5 provides the summary and overall conclusions.

2 Methods

2.1 The TSMP modelling platform

TSMP is a scale-consistent, highly modular, fully integrated soil-vegetation-atmosphere regional climate system model (e.g., Shrestha et al., 2014; Gasper et al., 2014). TSMP consists of three component models: the atmospheric Consortium for Small Scale Modelling (COSMO) model version 5.01, the Community Land Model (CLM) version 3.5, and the hydrological model ParFlow version 3.2. The component models are externally coupled via the Ocean Atmosphere Sea Ice Soil (OASIS) Model Coupling Toolkit (MCT) version 3.0 (Valcke, 2013), which enables interactions between different compartments of the geocosystem, explicitly reproducing feedbacks in the hydrological cycle from the bedrock into the atmosphere.

COSMO is a non-hydrostatic limited-area atmospheric model (Baldauf et al., 2011). It is based on the primitive thermohydrodynamical Euler equations formulated in rotated geographical coordinates and generalized terrain-following height coordinates, describing compressible flow in a moist atmosphere. COSMO parameterization schemes cover various physical processes, such as radiation, cloud microphysics, deep convection, etc. The boundary conditions for COSMO are provided

by a coarse grid model, i.e., reanalysis or GCM, whereas the lower boundary conditions (e.g., surface albedo, energy fluxes, surface temperature, surface humidity) are provided by CLM in the current TSMP configuration.

CLM is a biogeophysical model of the land surface (Oleson et al., 2004, 2008). It simulates land-atmosphere exchanges in response to atmospheric forcings. CLM consist of four components that describe biogeophysics, hydrologic cycle, biogeochemistry, and dynamic vegetation. In TSMP, CLM receives short-wave radiation, wind speeds, barometric pressure, precipitation, near-surface temperature, and specific humidity from COSMO. In turn, CLM sends infiltration and evapotranspiration fluxes for each soil layer of the ParFlow hydrological model.

ParFlow is a hydrological model that simulates variably saturated three-dimensional subsurface hydrodynamics using Richards equation integrated with shallow overland flow based on a kinematic wave approximation (Maxwell and Miller, 2005; Kollet and Maxwell, 2006; Kuffour et al., 2020). ParFlow allows 3D-redistribution of subsurface water in a continuum approach. In the TSMP set-up used, ParFlow replaces the hydrological functionality of CLM.

The evaluation run of TSMP was performed by Furusho-Percot et al. (2019), with atmospheric forcings derived from the ERA-Interim reanalysis, and was validated by comparing temperature and precipitation with E-OBS and column water storage with the Gravity Recovery and Climate Experiment (GRACE) satellite data (Landerer et al., 2020). In the recent publication of Ma et al. (2022), the TSMP water table simulation results were used in a machine learning approach and compared to in-situ water table observation anomalies over Europe; the results showed good agreement considering that TSMP model has not been calibrated.

2.2 The TSMP simulation set-up

TSMP simulations are conducted for the historical time period from December 1949 to the end of 2005 over the European domain according to the CORDEX simulation protocol (Gutowski et al., 2016) using rotated latitude-longitude model grid with a horizontal resolution of 0.11° (EUR-11) or about 12.5 km. CLM and ParFlow are initialised with the moisture conditions of the 1st of December 2011 from the TSMP evaluation run (Furusho-Percot et al., 2019). The COSMO configuration resembles that of the COSMO model in CLimate Mode (CCLM) (Rockel et al., 2008). COSMO extends vertically up to 22 km, divided into 50 levels. CLM has 10 soil layers with a total depth of 3 m, which coincide with the 10 top layers of ParFlow. ParFlow has in addition 5 bedrock layers increasing in thickness towards the bottom of the model domain to a total depth of 57 m. The time step for ParFlow and CLM is 900 sec, for COSMO it is 75 sec. The coupling time step between TSMP component models is 900 sec. The TSMP output constitutes terrestrial essential climate variables with a time step of 3 hours (https://datapub.fz-juelich.de/slts/regional_climate_tsmp_hi-cam/). The first 10 years of TSMP simulations are discarded due to hydrodynamic spin-up.

Forcing data for COSMO are provided by the Max-Planck Institute's MPI-ESM-LR r1i1p1 CMIP5 GCM with a resolution of T63L47 (Giorgetta et al., 2013). For CLM, plant functional types (PFT) are taken from the Moderate Resolution Imaging Spectroradiometer (MODIS) land cover dataset (Friedl et al., 2002). Leaf area index, stem area index, monthly bottom and top heights of each PFT are calculated based on the global CLM surface dataset (Oleson et al., 2008). Topography in ParFlow is represented by slopes estimated from the United States Geological Survey GTOPO30 (Daac, 2004). In this study,

155 we improved the representation of subsurface hydrogeology in ParFlow, compared to the previous work of Furusho-Percot
 et al. (2019, 2022), where the soil parameters were assumed to be vertically homogenous. Here, an aquifer network is added
 to ensure the relationship between surface and subsurface water flow (Naz et al., 2023). The land surface static input data,
 including soil properties (i.e., soil color, percentage clay and sand), dominant land use type, dominant soil types in the top
 160 datasets, namely: the Food and Agriculture Organization soil database (FAO, 1988), the pan-European River and Catchment
 Database (Vogt et al., 2007), International Hydrogeological map of Europe (IHME) (Duscher et al., 2015), and GLocal HY-
 drogeology MaPS (GLHYMPS) (Gleeson et al., 2014). The information on subsurface aquifers is derived from IHME. The
 soil parameters in the middle and upper layers (i.e., the top 10 ParFlow layers) are estimated based on the soil texture from
 the FAO database. The bedrock geology is constructed from the IHME hydrogeological information and the lower resolution
 165 GLHYMPS, in combination with the pan-European River and Catchment Database. The pan-European River and Catchment
 Database serves as a proxy for the alluvial aquifer system in ParFlow, assumed to lie underneath or near existing rivers.

2.3 Multi-model GCM-RCM ensemble

RCMs driven by CMIP5 GCMs control simulations (r1i1p1 ensemble members) over the European domain at EUR-11 hori-
 zontal resolution from the CORDEX experiment are used in conjunction with the coupled TSMP modelling platform to study
 170 the impact of 3D groundwater dynamics on the statistics of heat events. Note that CMIP5 GCM historical control simulations
 are performed under observed natural and anthropogenic forcing (e.g., Taylor et al., 2012).

In this study, based on availability, the following CORDEX ensemble members are considered, identified by their institu-
 tions: CLMcom (CCLM4-8-17 forced by MPI-ESM-LR and CNRM-CM5), CLMcom-ETH (COSMO-crCLIM forced by MPI-
 ESM-LR, CNRM-CM5, and NCC-NorESM1-M), MPI-CSC (REMO2009 driven by MPI-ESM-LR), GERICS (REMO2015
 175 forced by NCC-NorESM1-M, NOAA-GFDL-ESM2G, and IPSL-CM5A-LR), see Table 1 for details. Such a multi-model
 GCM-RCM ensemble includes two main groups of RCMs, namely COSMO and REMO in different versions, and 5 different

Table 1. The matrix of the GCM-RCM climate change scenario control runs.

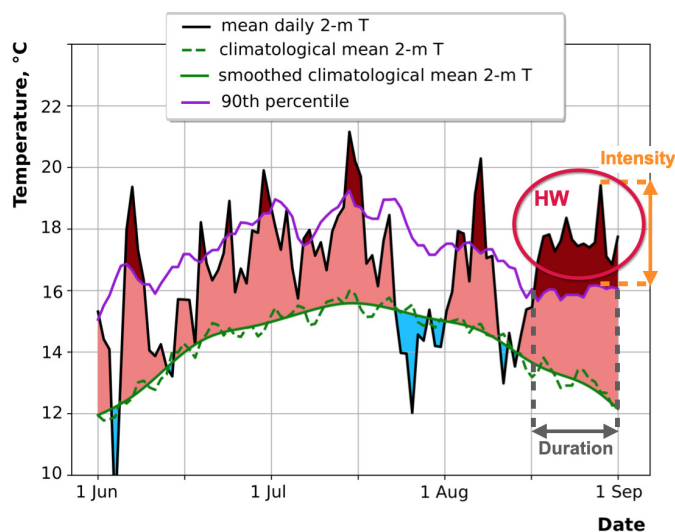
GCM-RCM	MPI-ESM-LR <i>(Giorgetta et al., 2013)</i>	CNRM-CM5 <i>(Voldoire et al., 2013)</i>	NCC-NORESM1-M <i>(Bentsen et al., 2013)</i>	NOAA-GFDL-ESM2G <i>(Dunne et al., 2012)</i>	IPSL-CM5A-LR <i>(Dufresne et al., 2013)</i>
TSMP <i>(Shrestha et al., 2014)</i>	X				
CCLM4-8-17 <i>(Rockel et al., 2008)</i>	X	X			
COSMO-crCLIM <i>(Pothapakula et al., 2020)</i>	X	X	X		
REMO2009 <i>(Jacob and Podzun, 1997)</i>	X				
REMO2015			X	X	X

GCMs, for a total of 10 different GCM-RCM pairs. TSMP is most compatible with CCLM4-8-17, with the main differences in the COSMO lower boundary condition: in TSMP, the lower boundary condition accounts for groundwater feedbacks due to the coupling between the land surface model CLM and the hydrological model ParFlow, unlike in CCLM4-8-17, where the soil processes are modelled by TERRA-ML, the soil-vegetation land surface model of COSMO (e.g., Grasselt et al., 2008; Schlemmer et al., 2018). With the exception of TSMP, the RCMs in the considered ensemble lack closure of water and energy cycles due to simplifications of the representation of subsurface hydrodynamics.

2.4 Detection and analysis of heat events

There is no universally accepted method, but the most commonly used approach to detect a heat event is based on a percentile temperature threshold (e.g., Zhang et al., 2005, 2011; Sulikowska and Wypych, 2020). However, temperature-based diagnostics are often ambiguous or inconsistent, and only partially describe heat events (Perkins and Alexander, 2013).

In this study, we determine a day with a daily mean temperature above the local 90th percentile of the reference period as a hot day. We calculate the 90th percentile for every summer day and for each EUR-11 grid point of the CORDEX European



Heat event #	Start date	End date	Duration, days	Intensity, °C
1.	1.06	1.06	1	0,26
2.	6.06	9.06	4	2,71
3.	19.06	19.06	1	1,30
4.	24.06	24.06	1	1,07
5.	30.06	1.07	2	1,40
6.	7.07	7.08	2	0,41
7.	15.07	17.07	3	1,90
8.	3.08	4.08	2	0,63
9.	6.08	7.08	2	3,08
10.	17.08	31.08	15	3,28

Figure 1. Schematic of a summer heat wave (HW) detection. An example is given for June-July-August of 1972 for one grid element [250, 300] of the CORDEX European domain. Data taken from the TSMP simulations. The solid black line is the daily mean 2 m air temperature for the summer season of 1972. The dashed green line shows the climatological daily mean 2 m air temperature calculated from the reference period 1961-1990, and the solid green line is its smoothing with a Butterworth filter. The solid violet line represents the 90th percentile of the daily mean 2 m air temperature calculated from a 5-day window centered on each summer calendar day of the reference period 1961-1990. The shaded light red colour indicates days with temperatures above the climatological mean, and the shaded dark red colour highlights days with temperatures above the 90th percentile. The characteristics of the heat events (start and end date, duration, intensity) detected during the considered summer season are also given.

190 domain from a consecutive 5-day moving window centered on that calendar day, from the 30-year reference period between 1961 and 1990, in each considered RCM. The first occurrence of a hot day defines the beginning of a heat event. A series of hot days constitutes a heat event, highlighted in dark red in Fig. 1. A heat event is interrupted if the daily mean temperature drops below the 90th percentile-based threshold.

A heat event can be characterised by its duration, intensity, and frequency (e.g., Horton et al., 2016). A heat event duration is the number of consecutive days over which the heat event lasts. If a heat event lasts long enough, it can be classified as a heat wave. Similar to Fischer and Schär (2010), we define a heat wave as a spell of at least six consecutive days with daily mean 2 m air temperatures above the local 90th percentile of the reference 1961-1990 period, see Fig. 1. Note that throughout this article, we consistently use the terms “hot day”, “heat event”, and “heat wave”. The total number of hot days during the investigated period corresponds to the TG90p heat index from the joint CCI/CLIVAR/JCOMM Expert Team on Climate Change Detection and Indices (ETCCDI) (Alexander et al., 2006), and describes the number of days with $TG_{ij} > TG_{in,90}$, where TG_{ij} is a daily mean temperature on day i of the investigated period j , and $TG_{in,90}$ is the 90th percentile calculated for day i from the 30-year reference period n .

A heat event intensity is the maximum of the difference between the daily mean temperature and the 90th percentile of the reference period within a single heat event (e.g., Vautard et al., 2013). Intensity represents the severity of a heat event (see Fig. 1). Adopting the definition of the Heat Wave Duration Index (HWDI) from Frich et al. (2002), in this study we classify a heat wave as intense if its intensity is at least 5 K. In literature, there are other classifications of heat waves depending on their intensity, for example, low, severe and extreme (Nairn and Fawcett, 2014), or weak, moderate and intense (Lhotka and Kyselý, 2015).

A frequency of heat events of a certain type (e.g., of a certain duration or intensity) over the investigated period is the number of these heat events divided by the total number of all heat events that occurred during the period under study (e.g., Vautard et al., 2013). For example, in Fig. 1 heat events with a duration of 2 days occur 4 times, while the total number of all heat events is equal to 10. Therefore, the resulting frequency of 2-day heat events during the summer of 1972 for the considered grid element is 0.4, indicating that 40% of all heat events are 2 days in duration.

215 3 Results

In the following we examine the groundwater representation on the distribution of simulated heat events in RCMs. In particular, we investigate whether the new dataset from TSMP driven by MPI-ESM-LR is consistent with the CORDEX GCM-RCM ensemble of climate change scenario control runs (see Table 1) and seek to gain insight into the role of an explicit representation of groundwater in long-term climate simulations over Europe. We assess the statistics of the characteristics of heat events, i.e., their duration, intensity, and frequency, from daily mean 2 m air temperatures on the native EUR-11 grid. The analysis is conducted in the focus domain (Fig. 2), which covers the European continent [10°W-30°E, 36°N-70°N]. The analysis is carried out for the summer season of the 30-year period from 1976 to 2005 with respect to the reference period 1961-1990 in each RCM. Note that grid elements belonging to the ocean are omitted from the analysis.

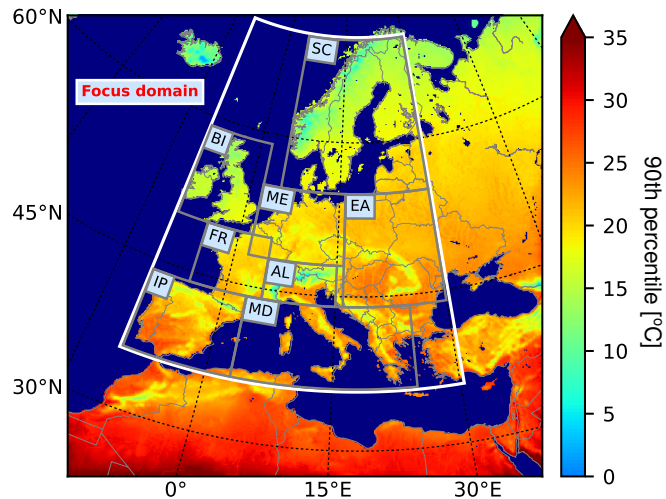


Figure 2. Mean 90th percentile of 2 m air temperatures from TSMP simulations for the summer season of the 1961-1990 period. The white box indicates a focus domain [10°W-30°E, 36°N-70°N] used in the analysis. PRUDENCE regions are shown with grey boxes: British Isles (BI), Iberian Peninsula (IP), France (FR), Mid-Europe (ME), Scandinavia (SC), Alps (AL), Mediterranean (MD) and Eastern Europe (EA).

3.1 Number of hot days

225 We examine the impact of groundwater dynamics on the interannual variability of the occurrence of hot days during the summer seasons from 1976 to 2005 with regard to the reference period 1961-1990 in each RCM (see Fig. 2). A comparison of the time series of the number of hot days, that is the TG90p index, in summer averaged over the focus domain, i.e., over the total number of land grid elements in the focus domain, shows that the impact of an explicit representation of groundwater dynamics in RCMs varies from year to year (Fig. 3). The summer TG90p index averaged over the focus domain between 1976
 230 and 2005 results in 10.95 days in the TSMP simulations and 11.64 days in the CORDEX multi-model ensemble average (see Fig. 3). A positive linear trend in the summer mean TG90p index is observed in all considered RCMs, with the decadal change in the TSMP simulations being 1.53 days, while this value averaged over the CORDEX ensemble reaches 1.99 days.

The spatial distributions of the seasonal mean, variability, and decadal change of the summer TG90p index are shown in Fig. 4-6. There, the spatial patterns from RCMs driven by the same GCMs show rather similar behaviour, indicating that the
 235 climatological occurrence of summer hot days is largely controlled by the large-scale atmospheric circulation imposed by the GCM boundary conditions. TSMP produces the smoothest spatial distribution of the seasonal mean and variability of the summer TG90p index compared to the CORDEX ensemble (see standard deviations in Fig. 4, 5). The mean and interannual variability of the summer TG90p index averaged over the focus domain are also lowest in TSMP compared to the CORDEX ensemble (Tables A1, A2 in Appendix A).

240 The TSMP-simulated summer TG90p index is consistent with that of the RCMs driven by MPI-ESM-LR from the CORDEX ensemble, although there are some regional differences (see Fig. 4a-d, Fig. 5a-d, Fig. 6a-d). The largest differences occur in

the Iberian Peninsula PRUDENCE region, with TSMP yielding the lowest values: summer mean TG90p index is equal to 10.36 days in TSMP and ranges from 12.54 days to 12.75 days in the CORDEX RCMs driven by MPI-ESM-LR, variability of the summer TG90p index reaches 6.17 days in TSMP and ranges from 8.01 days to 9.59 days in the CORDEX RCMs driven by MPI-ESM-LR, and decadal change of the summer TG90p index is 2.26 days in TSMP and ranges from 3.66 days to 4.25 days in the CORDEX RCMs driven by MPI-ESM-LR (see Appendix A). As for the decadal change, the RCMs driven by MPI-ESM-LR show a positive trend in Southern and Central Europe and a negative trend in Northern Europe. Note that there is no unequivocal agreement in the decadal change at the entire GCM-RCM ensemble considered, yet the decadal trend of the summer TG90p index averaged over the focus domain is positive in all models of the investigated GCM-RCM ensemble, reaching values between 1.13 days and 2.71 days (see Table A3 in Appendix A).

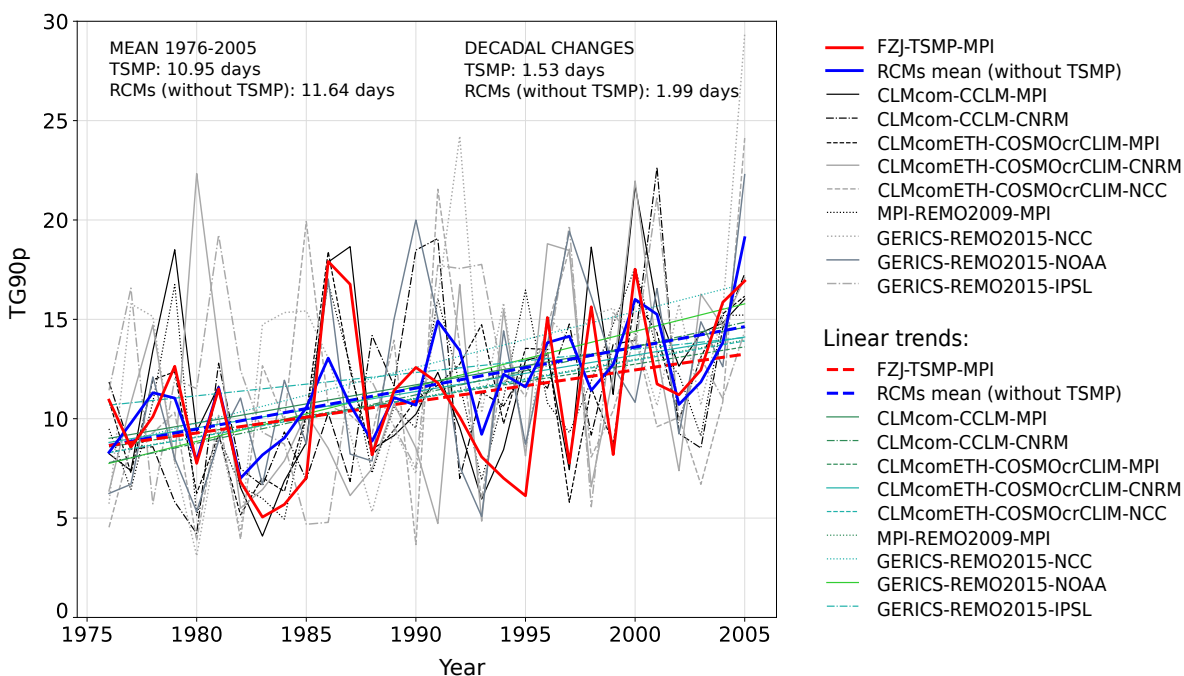


Figure 3. Time series and linear trends of the summer mean TG90p index, averaged over the focus domain, during 1976-2005 with respect to the reference period 1961-1990, in the TSMP simulations and the CORDEX ensemble. The solid and dashed red lines show the summer mean TG90p index and its linear trend from the TSMP simulations. The black and grey lines represent the summer mean TG90p index from the CORDEX ensemble and the green lines are their linear trends, respectively. The summer mean TG90p index averaged over the CORDEX multi-model ensemble is shown with the solid blue line, and its linear trend is shown with the dashed blue line.

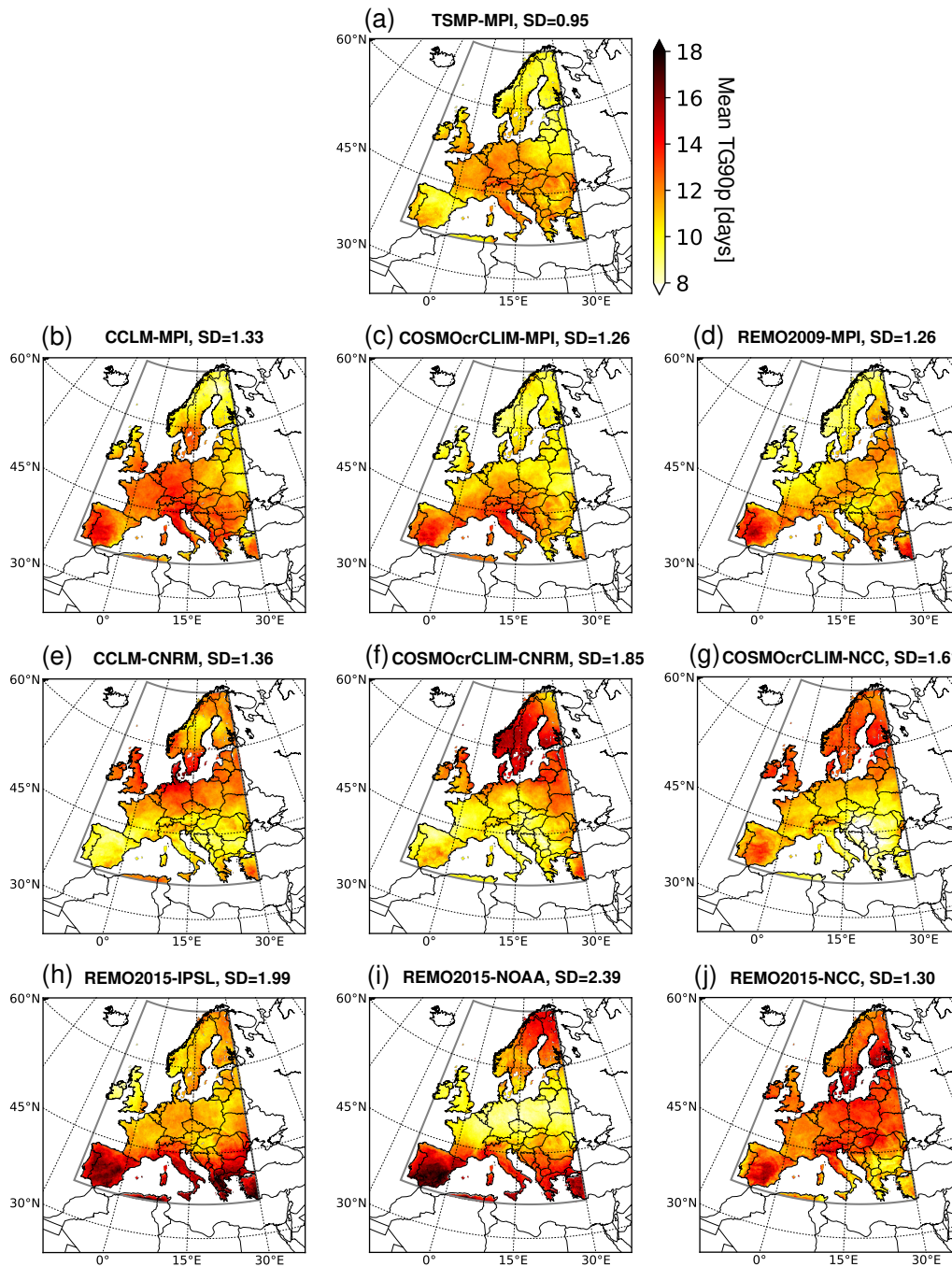


Figure 4. Spatial distribution of the summer TG90p index averaged between 1976 and 2005 in TSMP (a) and the CORDEX ensemble (b-j). A standard deviation (SD) of the spatial distribution of the summer mean TG90p is indicated in every figure.

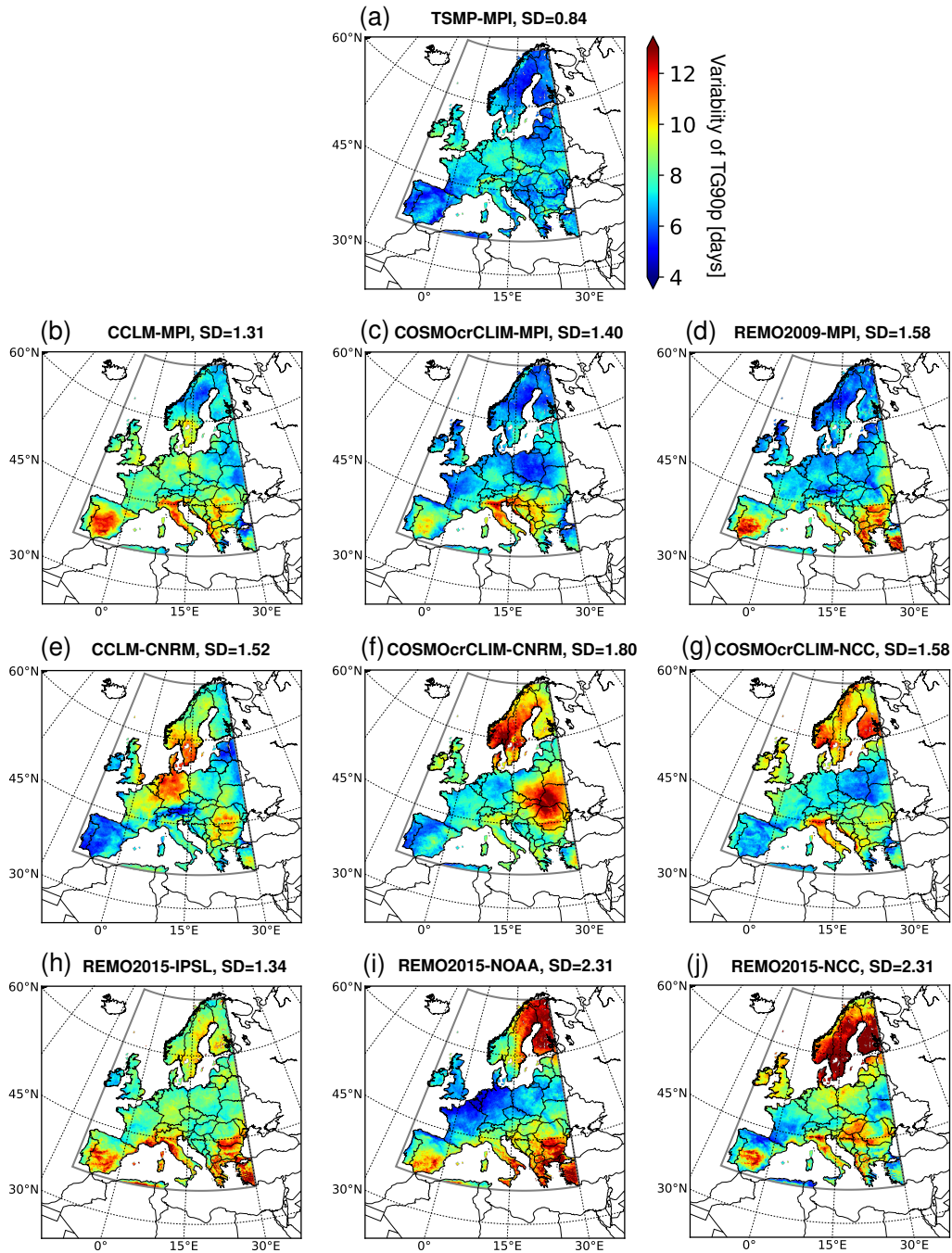


Figure 5. Variability of the summer TG90p index, calculated for each grid element from the time series of the summer mean TG90p index between 1976 and 2005 as standard deviation, for TSMP (a) and the CORDEX ensemble (b-j). A standard deviation (SD) of the spatial distribution of the variability of the summer mean TG90p index is indicated in every figure.

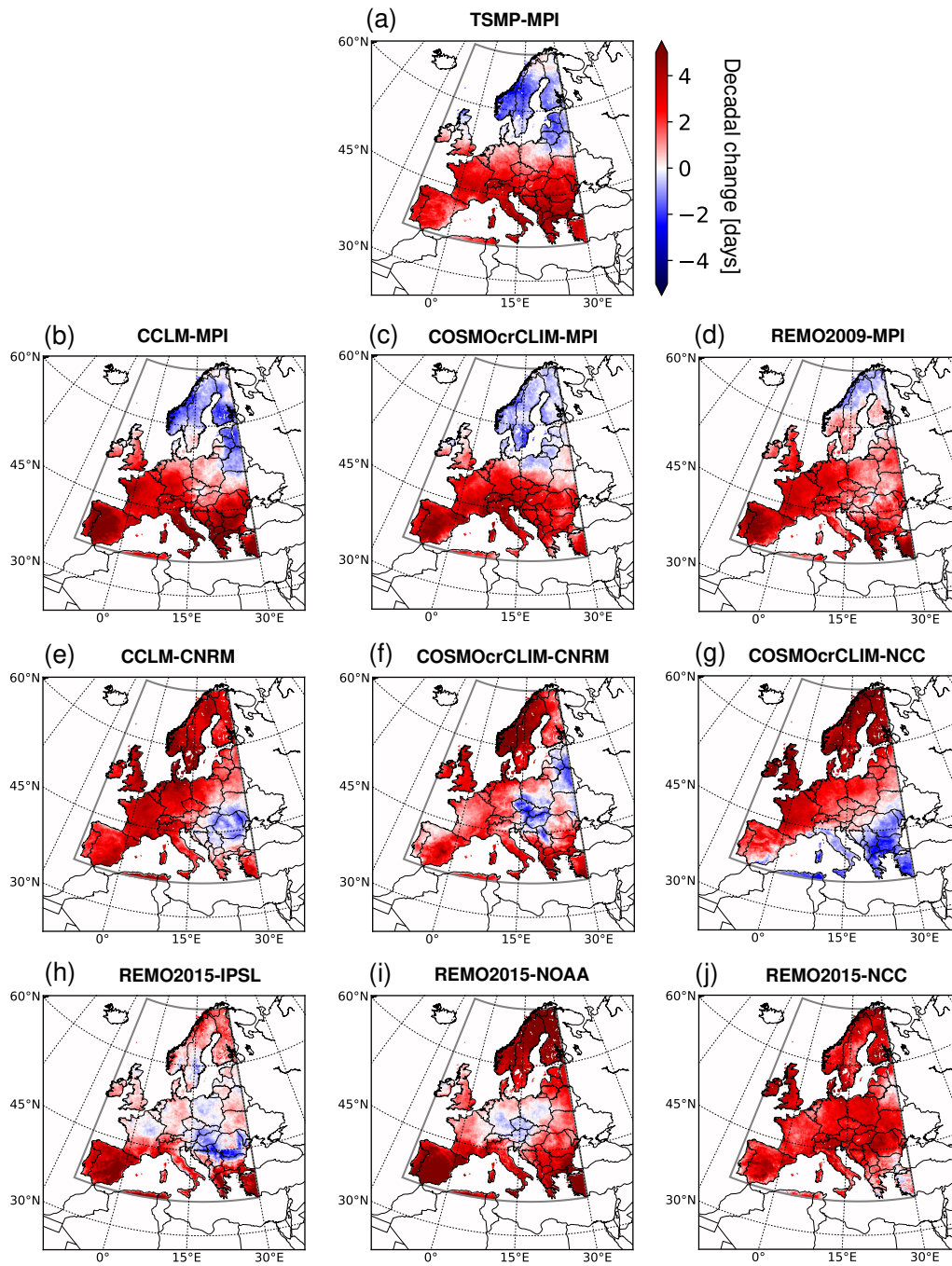


Figure 6. Spatial distribution of the decadal change in the summer TG90p index, calculated for each grid element from the time series of the summer mean TG90p index between 1976 and 2005 as a linear trend, for TSMP (a) and the CORDEX ensemble (b-j).

255 3.2 Heat events of different durations

The summer seasonal number of heat events (i.e., series of consecutive hot days) of different durations that occur on average over the focus domain between 1976 and 2005 is shown in Fig. 7a. In the considered GCM-RCM multi-model ensemble, the mean number of heat events of any duration per summer in the focus domain ranges from 4.18 to 4.86 heat events, with TSMP simulating 4.66 heat events. The ratio of the number of heat events between the CORDEX RCMs and TSMP (see blue lines
260 in Fig. 7a) is greater than 1 for heat waves, i.e., heat events lasting at least 6 days, and increases towards the heat waves of long durations. This behaviour indicates that TSMP systematically simulates the least number of heat waves compared to the CORDEX ensemble. An intercomparison of the CORDEX RCMs shows that COSMO tends to simulate fewer heat waves compared to REMO.

The GCM-RCM multi-model ensemble leads to different spatial distributions of heat waves (Fig. 8). TSMP generates the
265 smoothest spatial distribution of the number of heat waves, resulting in the smallest regional differences compared to the CORDEX ensemble (see indicated standard deviations in Fig. 8). The decadal number of summer heat waves is between 3.25 and 5.09 in the GCM-RCM multi-model ensemble, with the lowest value in TSMP (Table B1 in Appendix B). When comparing TSMP with the CORDEX RCMs driven by MPI-ESM-LR, the TSMP simulation has most of the heat waves located in Central Europe, while the RCMs from the CORDEX ensemble simulate the highest number of heat waves towards Southern Europe.
270 The largest differences occur in the Iberian Peninsula, with 2.51 heat waves per decade in TSMP and between 4.88 and 5.25 heat waves per decade in the RCMs driven by MPI-ESM-LR from the CORDEX ensemble.

The contribution of heat waves to the total number of hot days is presented in Fig. 9. Here, heat waves account for from 22.38 % to 34.40 % of hot days, on average in the focus domain, with TSMP giving the lowest value (Table B2 in Appendix B). The highest fraction of hot days attributed to heat waves prevails in Scandinavia, from 26.50 % to 39.04 %, while Eastern
275 Europe tends to be the region with the lowest number of hot days associated with heat waves, from 16.27 % to 38.21 %, in the GCM-RCM multi-model ensemble. From the comparison of TSMP with the RCMs driven by MPI-ESM-LR, the largest differences in the proportion of hot days belonging to heat waves are observed in the Iberian Peninsula, where TSMP simulates 17.47 % and the RCMs driven by MPI-ESM-LR from the CORDEX ensemble simulate from 31.19 % to 33.04 %.

280 3.3 Heat waves of different intensities

The dependence of the frequency of heat waves occurring in the focus domain between 1976 and 2005 on their intensities is
285 shown in Fig. 7b. The maximum frequency of heat waves is equal to 1 for an intensity greater than 0 in all RCMs, because for each RCM all heat waves from the focus domain, that occur between 1976 and 2005, are taken into account. The ratio of heat wave frequencies between the CORDEX RCMs and TSMP (see blue lines in Fig. 7b) increases towards intense heat waves, i.e., heat waves with an intensity of at least 5 K, except for REMO2015 driven by IPSL-CM5A-LR. TSMP shows a systematic behavior to simulate less intense heat waves on average in the focus domain compared to the CORDEX ensemble. Note that
290 the largest discrepancy in the frequency of heat waves with TSMP is found in CCLM4-8-17 driven by MPI-ESM-LR, up to a factor of 12 or even more depending on the intensity considered, although TSMP is the most compatible with CCLM4-8-17

in the considered GCM-RCM multi-model ensemble. An intercomparison of the RCMs within the CORDEX ensemble shows that COSMO tends to simulate more intense heat waves than REMO.

The most intense heat waves are located in Western and Northern Europe in the majority of RCMs of the considered multi-model ensemble (Fig. 10). The frequency of intense heat waves occurring in the focus domain between 1976 and 2005 ranges from 0.174 to 0.301, i.e., from 17.4% to 30.1% heat waves are intense in the GCM-RCM multi-model ensemble, with TSMP giving the second lowest value after REMO2015 driven by IPSL-CM5A-LR (Table B3 in Appendix B). As already noted, TSMP has the largest discrepancy in the frequency of heat waves with CCLM4-8-17 driven by MPI-ESM-LR, with particularly large differences in the France PRUDENCE region, where TSMP leads to a frequency of 0.246 and CCLM4-8-17 to 0.468. It

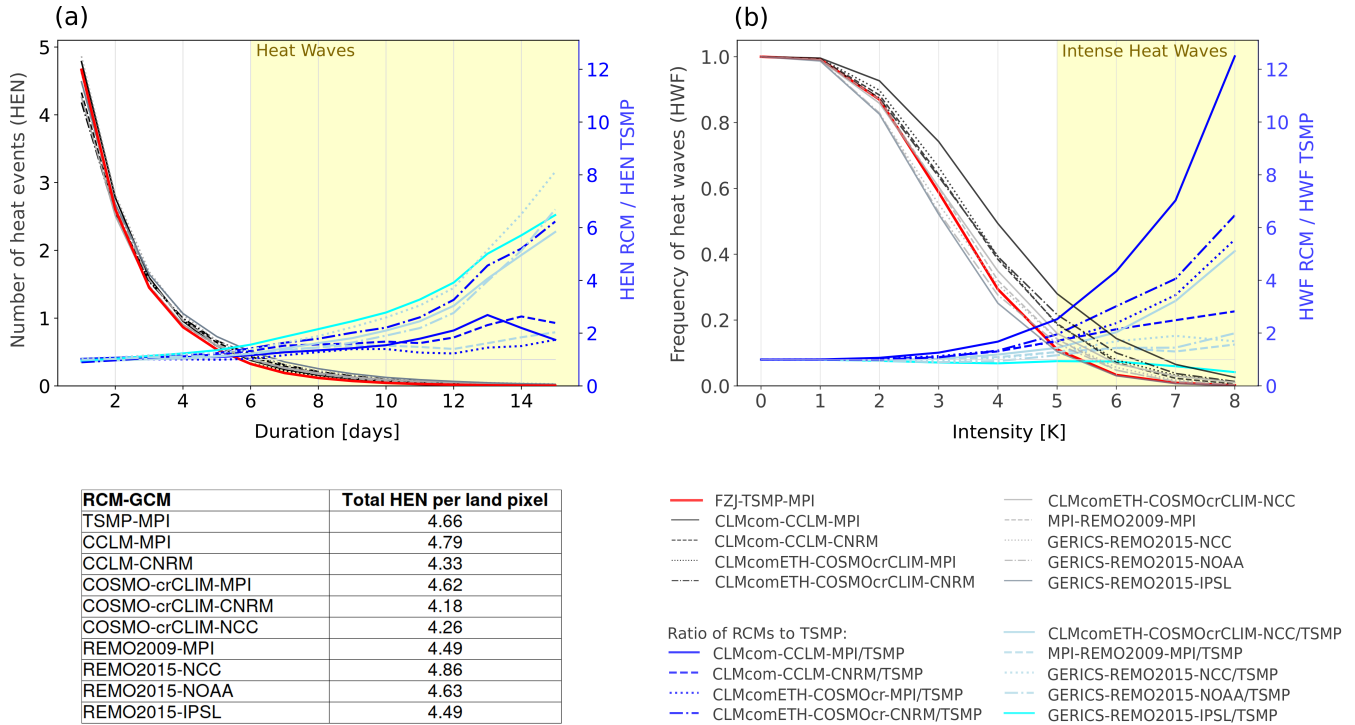


Figure 7. (a) Mean number of summer heat events (HEN, y-axis) of duration equal to or greater than a given number of days (x-axis) as a function of this number of days. The averaging is performed over the focus domain and the total number of investigated years, i.e., 30 years, from 1976 to 2005. HEN is shown with the red solid line for TSMP and with the black and grey lines for the CORDEX ensemble. The total HEN occurring on average annually over the focus domain during the summer season in the GCM-RCM ensemble is given in the table. (b) Frequency of heat waves (HWF, y-axis) with intensities equal to or higher than a value indicated on the abscissa, that occur in the focus domain from 1976 to 2005, as a function of the intensity. HWF is shown with the red solid line for TSMP and with the black and grey lines for the CORDEX ensemble. Panels (a) and (b) also show the ratio of HEN and HWN values between RCMs from the CORDEX ensemble and TSMP, represented by the blue lines. Data are taken from the summer seasons between 1976 and 2005 with respect to the reference period 1961-1990 in each RCM. The representation of the dependencies is adopted from the work of Vautard et al. (2013).

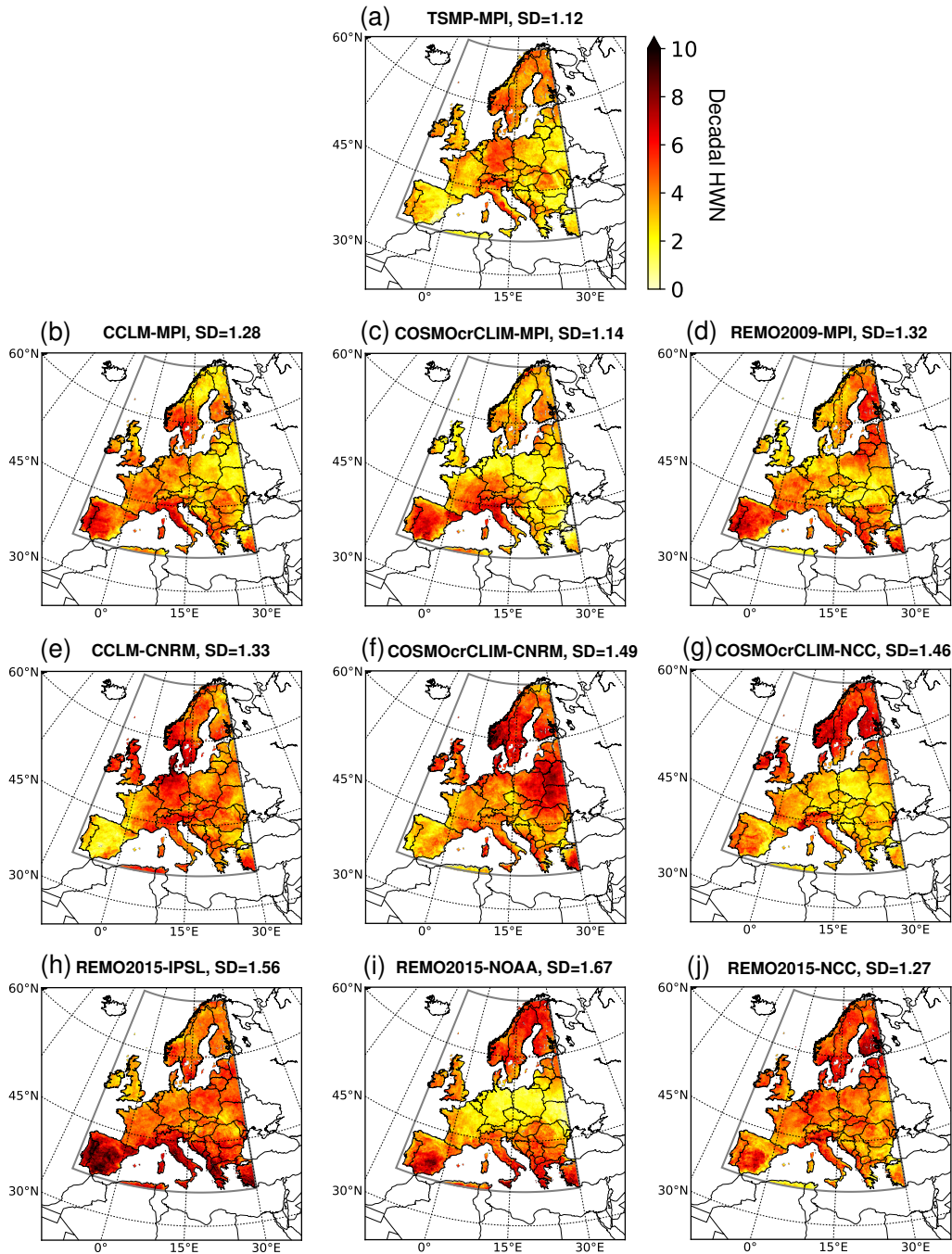


Figure 8. Spatial distribution of the decadal number of heat waves (HWN) in summer, calculated from the data between 1976 and 2005 with respect to the reference period 1961-1990, for TSMP (a) and the CORDEX ensemble (b-j). A standard deviation (SD) of the spatial distribution of the decadal HWN is indicated in every figure.

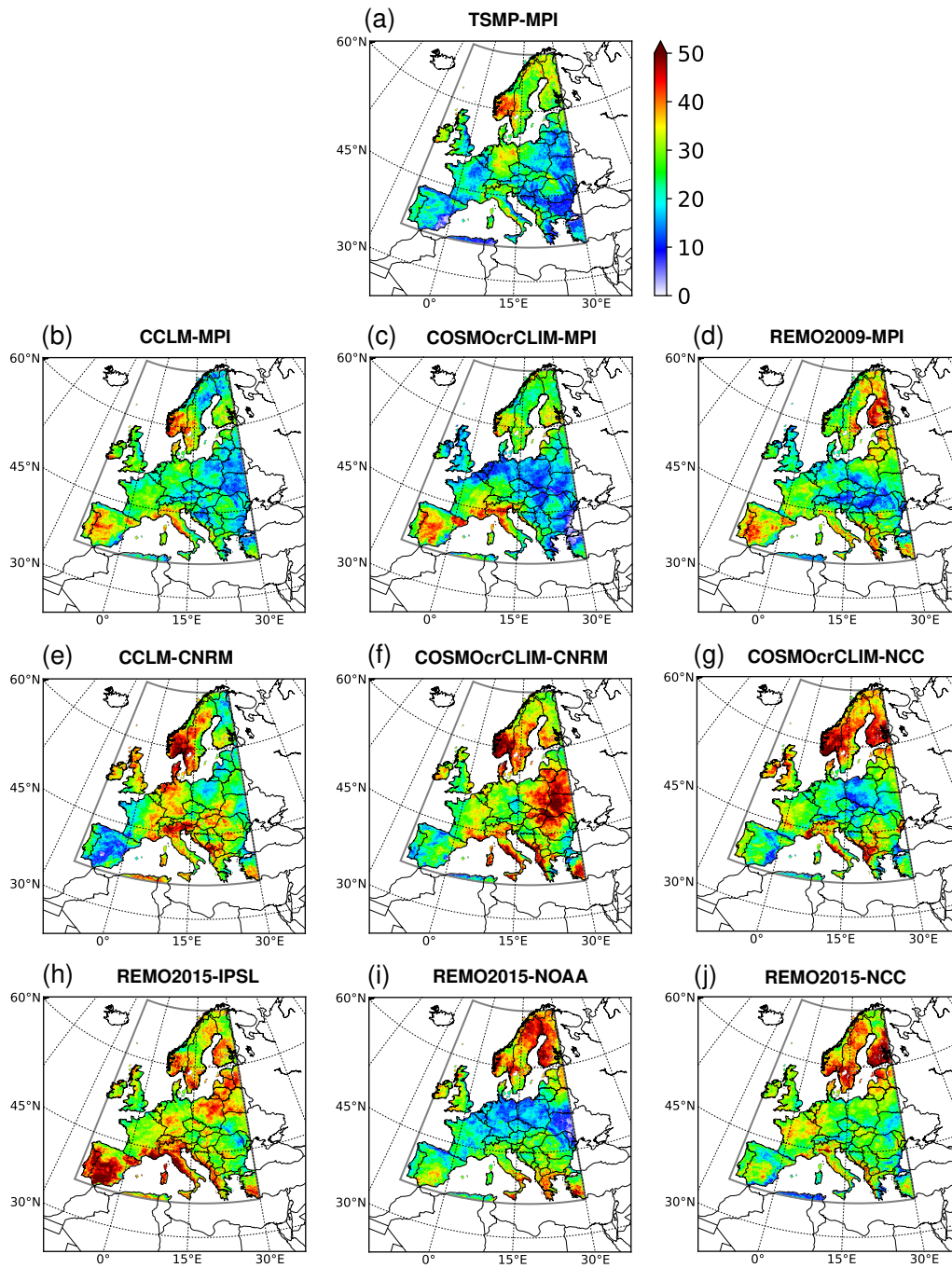


Figure 9. Contribution of heat waves to the number of hot days [%], calculated from the total number of heat waves and hot days accumulated between 1976 and 2005, for TSMP (a) and the CORDEX ensemble (b-j)

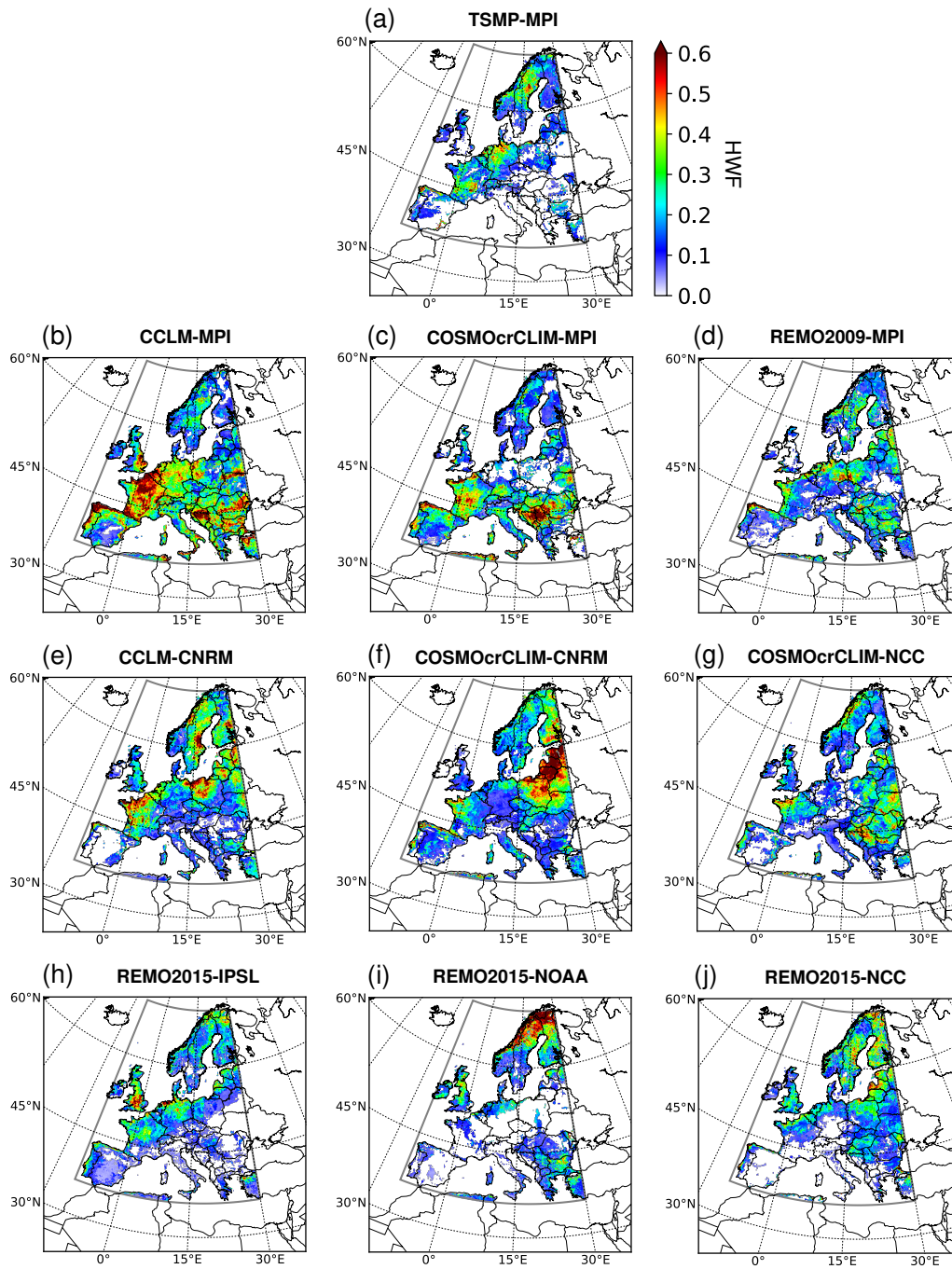


Figure 10. Frequency of intense heat waves (HWF), i.e., heat waves with intensities of at least 5 K, relative to the total number of heat waves occurring between 1976 and 2005 in each RCM. The HWF distribution is shown for TSMP (a) and the CORDEX ensemble (b-j).

300 is important to point out that the regions with the highest number of intense heat waves do not necessarily coincide with the regions that experience the most heat waves. The origin of such behaviour should be further investigated and is beyond the scope of this analysis.

4 Discussion

4.1 Physical mechanisms

305 Compared to the simplified 1D free drainage approach, the 3D physics-based groundwater representation in TSMP leads to regionally shallow groundwater levels, causing wetter soils (Keune et al., 2016). This leads to an increase in evapotranspiration by an increase in the latent heat flux and a decrease in the sensible heat flux (Maxwell and Condon, 2016). In turn, higher evapotranspiration causes moistening of the lower atmosphere and increases downward longwave radiation due to the greenhouse effect of water vapor, on the other hand, it causes cooling of the surface and reduces outgoing surface longwave
310 radiation (e.g., Pal and Eltahir, 2001; Yang et al., 2018). Additionally, higher evapotranspiration may lead to moist convection or rainfall, which further affects soil moisture. As result, TSMP simulates a more consistent spatial and temporal distribution of soil moisture (Keune et al., 2016). The simplified representation of groundwater dynamics in RCMs leads to the opposite effect, i.e., deeper groundwater levels and drier soils, overestimating the coupling between the land surface and the atmosphere. This causes a decrease in cloud cover and an enhancement of net solar radiation, thus increasing near-surface temperatures,
315 which further reduces soil moisture (e.g., Vogel et al., 2018; Hartick et al., 2022).

The results of our study suggest that the response of summer heat events to an explicit representation of groundwater dynamics in TSMP within the considered GCM-RCM multi-model ensemble varies from year to year (see Fig. 3). Incorporated 3D groundwater dynamics in TSMP accounts for long-term soil moisture memory effects (Hartick et al., 2021), unlike the RCMs from the CORDEX ensemble. Soil moisture memory contributes to either increasing the probability of a subsurface
320 water storage deficit in regions that have had a subsurface water deficit in the previous year due to drought conditions, thereby increasing the occurrence of heat events, or, conversely, buffering droughts and reducing the number of heat events (e.g., Martínez-de la Torre and Miguez-Macho, 2019; Hartick et al., 2021; Dirmeyer et al., 2021). Droughts can also remotely affect areas outside the drought region through changes in atmospheric circulation and advection of air masses and further contribute to the evolution of heat events (Fischer et al., 2007).

325 Considering an extended period of 30 years, TSMP driven by MPI-ESM-LR shows systematic differences in the distribution of the heat events characteristics (i.e., duration, intensity, frequency) compared to the CORDEX ensemble, by simulating fewer, shorter, and less severe heat events in Europe with smaller regional differences. We relate this behaviour to a more realistically simulated soil moisture and, thus, evapotranspiration, in TSMP (see also Furusho-Percot et al., 2022). The tendency for different responses in different PRUDENCE regions can be explained by the soil moisture-temperature feedbacks associated
330 with evaporative regimes, namely energy-limited (i.e., a wet regime with the main control of land evaporation by incoming radiation) in Northern Europe and moisture-limited (i.e., a dry regime with increased or decreased land evaporation in response to increased or decreased soil moisture content) prevailing in Southern Europe (e.g., Seneviratne et al., 2010; Haghghi et al.,

2018; Jach et al., 2022). From the comparison of TSMP with the most compatible RCM from the CORDEX ensemble, i.e., CCLM4-8-17 forced by MPI-ESM-LR, an explicit representation of groundwater has a particularly strong impact on the intensity of heat waves versus their duration (see Fig. 7), the physical mechanisms of this phenomenon require further investigation and are beyond the scope of this study.

4.2 Methodology limitations

To capture the full range of divergence in the model performance over a historical period, and hence the potential uncertainties, within a multi-model GCM-RCM ensemble, it is necessary to combine as many different GCM-RCM as possible (e.g., Déqué et al., 2012; Christensen and Kjellström, 2020). Often some RCMs and GCMs are overrepresented over others, leading to conflicting results (Turco et al., 2013; Fernández et al., 2019). In general, the role of the GCM-imposed boundary conditions is greater than the role of RCMs in the multi-model GCM-RCM ensemble (e.g., Déqué et al., 2007; Evin et al., 2021). In this study, a limited number of GCM-RCM pairs (see Table 1) were used for a comparison with TSMP, and expanding the multi-model GCM-RCM ensemble or using other GCM-RCM pairs may lead to quantitatively different responses.

The GCM-RCM multi-model ensemble is not intended for direct comparison between individual models, as it includes different RCMs in combination with different driving GCMs. Therefore, due to the interplay of various factors (e.g., model set-up, conceptual and structural model uncertainties, different physical parameterizations, internal variability, boundary conditions, representation of the subsurface-land-atmosphere feedbacks, etc.) in addition to groundwater representation, it is challenging to reveal the exact cause-and-effect relationships between the explicit groundwater representation and simulated heat events. However, consideration of an extended period, e.g., 30 years between 1976 and 2005, allows to draw statistical conclusions.

To quantify the exact impact of the explicit representation of groundwater in TSMP and minimise the influence of other factors, it would be necessary to additionally carry out a long-term TSMP climate simulation with a simplified 1D free drainage approach for groundwater representation, and then compare the affected processes within TSMP rather than across the multi-model GCM-RCM ensemble. Since our study uses the same version of the TSMP model as in Keune et al. (2016), which have already shown the effects of 3D groundwater dynamics on the water and energy balance, and taking into account the high computational cost, the additional TSMP simulation with simplified groundwater representation is not conducted. Furthermore, the multi-model GCM-RCM ensemble study provides insight into the consistency between the new dataset of TSMP simulations forced by MPI-ESM-LR and the CORDEX ensemble.

Note that the results of this research are limited to the definitions of *hot day*, *heat event*, *heat wave*, *intense heat wave*, as well as the method of percentile estimation and the choice of the investigated and the reference time periods (see Sec. 2.4). For instance, Sulikowska and Wypych (2020) indicate that different variations of the metrics lead to a different distribution of hot days in summer in Europe.

5 Summary and conclusions

We presented a first-of-its-kind dataset of TSMP simulations driven by the CMIP5 MPI-ESM-LR GCM boundary conditions, in the context of dynamical downscaling of GCMs by RCMs for climate change studies. Unlike most RCMs, TSMP is a fully coupled regional climate system model with an explicit representation of groundwater. We investigated the role of groundwater representation for heat events in a multi-model GCM-RCM ensemble of 10 different GCM-RCM members, by comparing TSMP results and those from the CORDEX RCMs with simplified groundwater. Specifically, we performed a statistical analysis of the characteristics of heat events (i.e., duration, intensity, frequency) over Europe during the summer seasons between 1976 and 2005 with respect to the reference period 1961-1990 in each RCM.

The characteristics of heat events simulated by TSMP are consistent with the CORDEX ensemble, although there are systematic differences observed over the 30 years of simulations, which we attribute to an explicit representation of groundwater in TSMP. Our findings suggest that incorporated 3D groundwater dynamics in TSMP leads to a reduction in the number of hot summer days, their interannual variability and decadal change, and causes smaller regional differences, compared to the CORDEX ensemble. The representation of groundwater in TSMP also affects simulated heat waves distribution and leads to a reduction in the number of heat waves, as well as to a reduction in their duration and intensity, compared to the CORDEX ensemble. From the comparison of TSMP and the CORDEX RCMs driven by MPI-ESM-LR, the Iberian Peninsula is the most sensitive region to the groundwater representation.

This study clearly indicates that a coupled regional climate system model with 3D groundwater dynamics systematically simulates a different climatology of heat events in Europe compared to RCMs with simplified representation of groundwater. The results emphasize the importance of hydrological processes for reliable climate simulations and, in particular, for reducing biases in the duration, intensity and frequency of heat waves, and are of further importance when assessing uncertainties in climate change projections.

Appendix A: TG90p index in different regions of Europe

RCMs \ Regions	BI	IP	FR	ME	SC	AL	MD	EA	FD
TSMP-MPI	10.95	10.36	11.50	11.76	10.00	12.20	11.40	11.13	10.95
CCLM-MPI	11.49	12.64	12.46	12.80	10.42	13.27	12.62	11.50	11.80
COSMO-crCLIM-MPI	9.94	12.54	11.28	11.18	9.93	12.91	12.03	10.82	11.10
REMO2009-MPI	9.45	12.75	10.82	10.90	10.24	11.56	11.59	11.28	11.14
CCLM4-CNRM	12.89	9.66	10.93	12.62	12.06	10.74	10.49	11.16	11.32
COSMO-crCLIM-CNRM	12.05	10.14	9.87	10.87	13.87	10.15	9.85	11.26	11.46
COSMO-crCLIM-NCC	12.78	11.66	11.21	10.96	12.84	10.76	9.02	9.91	11.10
REMO2015-NCC	12.61	12.89	12.06	12.86	13.31	13.27	11.27	12.95	12.72
REMO2015-IPSL	9.56	15.00	11.45	11.48	11.29	12.64	15.25	11.63	12.38
REMO2015-NOAA	9.96	15.33	10.54	8.98	12.21	11.56	13.87	10.05	11.77

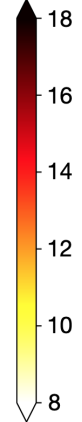


Table A1. Summer TG90p index [days] averaged between 1976 and 2005 in the GCM-RCM multi-model ensemble for the focus domain (FD, see Fig. 2) and the PRUDENCE regions: British Isles (BI), Iberian Peninsula (IP), France (FR), Mid-Europe (ME), Scandinavia (SC), Alps (AL), Mediterranean (MD), Eastern Europe (EA). Refer to Fig. 4 for the spatial distribution.

385

RCMs \ Regions	BI	IP	FR	ME	SC	AL	MD	EA	FD
TSMP-MPI	7.68	6.17	6.92	7.43	6.26	7.50	6.93	6.93	6.80
CCLM-MPI	8.50	9.59	8.30	8.53	7.45	8.82	9.34	8.02	8.33
COSMO-crCLIM-MPI	6.75	8.01	6.56	6.90	6.56	8.56	9.00	7.42	7.38
REMO2009-MPI	6.73	8.94	7.36	6.81	6.48	7.39	9.37	7.62	7.62
CCLM4-CNRM	8.07	6.37	8.72	10.00	8.47	7.32	8.28	8.17	8.21
COSMO-crCLIM-CNRM	8.50	6.84	7.38	7.42	10.22	8.38	8.19	10.31	8.90
COSMO-crCLIM-NCC	9.24	6.89	7.91	7.41	10.06	8.73	8.79	7.59	8.37
REMO2015-NCC	9.94	8.05	7.21	8.57	12.21	8.48	8.86	8.77	9.42
REMO2015-IPSL	7.74	9.51	8.16	8.39	8.94	9.60	10.13	8.40	8.97
REMO2015-NOAA	6.88	8.71	6.18	5.87	10.24	8.05	10.49	8.11	8.69

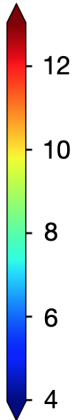


Table A2. Variability of the summer mean TG90p index [days], calculated from the data between 1976 and 2005 in the GCM-RCM multi-model ensemble, for the focus domain (FD, see Fig. 2) and the PRUDENCE regions: British Isles (BI), Iberian Peninsula (IP), France (FR), Mid-Europe (ME), Scandinavia (SC), Alps (AL), Mediterranean (MD), Eastern Europe (EA). Refer to Fig. 5 for the spatial distribution.

RCMs \ Regions	BI	IP	FR	ME	SC	AL	MD	EA	FD
TSMP-MPI	0.62	2.26	2.90	1.52	-0.98	3.33	3.74	1.84	1.53
CCLM-MPI	1.39	4.25	3.49	2.03	-0.89	3.29	4.40	1.21	1.86
COSMO-crCLIM-MPI	0.79	3.66	2.87	1.98	-0.62	4.02	2.86	1.47	1.68
REMO2009-MPI	1.80	3.69	3.29	2.67	0.15	2.50	2.65	1.29	1.88
CCLM4-CNRM	3.56	2.78	3.52	3.40	3.29	2.88	1.66	0.43	2.35
COSMO-crCLIM-CNRM	3.00	1.76	1.34	1.36	2.95	1.49	2.54	0.08	1.77
COSMO-crCLIM-NCC	4.50	1.58	3.56	2.43	4.09	1.32	-1.24	0.52	1.87
REMO2015-NCC	3.92	2.64	2.23	2.51	3.08	3.17	1.97	2.85	2.71
REMO2015-IPSL	0.55	3.89	0.57	0.23	0.87	1.27	2.22	-0.20	1.13
REMO2015-NOAA	1.11	5.18	1.44	0.13	4.27	1.27	3.49	1.16	2.68

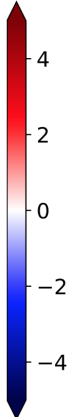


Table A3. Decadal change in the summer TG90p index [days], calculated from the data between 1976 and 2005 in the GCM-RCM multi-model ensemble, for the focus domain (FD, see Fig. 2) and the PRUDENCE regions: British Isles (BI), Iberian Peninsula (IP), France (FR), Mid-Europe (ME), Scandinavia (SC), Alps (AL), Mediterranean (MD), Eastern Europe (EA). Refer to Fig. 6 for the spatial distribution.

Appendix B: Characteristics of heat waves for different regions of Europe

390

RCMs \ Regions	BI	IP	FR	ME	SC	AL	MD	EA	FD
TSMP-MPI	3.33	2.51	3.15	4.01	3.83	4.13	3.04	2.74	3.25
CCLM-MPI	3.85	4.88	4.20	3.84	3.59	4.50	4.48	2.86	3.78
COSMO-crCLIM-MPI	2.54	4.99	3.73	2.78	3.46	5.27	3.59	2.34	3.35
REMO2009-MPI	2.70	5.25	4.17	3.30	4.17	3.50	4.40	3.24	3.89
CCLM4-CNRM	5.25	2.53	3.57	5.31	4.69	5.09	4.43	4.15	4.31
COSMO-crCLIM-CNRM	4.84	3.18	3.69	4.09	5.65	4.03	4.18	5.27	4.63
COSMO-crCLIM-NCC	5.24	3.66	3.86	3.15	5.61	4.10	3.43	2.92	3.97
REMO2015-NCC	4.42	4.23	4.15	4.64	5.52	4.69	3.92	4.01	4.49
REMO2015-IPSL	3.21	7.25	4.49	4.23	4.44	5.59	6.77	4.58	5.09
REMO2015-NOAA	3.91	4.93	3.10	2.02	5.03	3.57	5.42	2.62	3.95

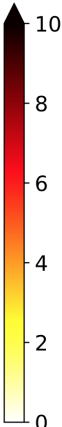


Table B1. Decadal number of summer heat waves, calculated from the data between 1976 and 2005 in the GCM-RCM multi-model ensemble, for the focus domain (FD, see Fig. 2) and the PRUDENCE regions: British Isles (BI), Iberian Peninsula (IP), France (FR), Mid-Europe (ME), Scandinavia (SC), Alps (AL), Mediterranean (MD), Eastern Europe (EA). Refer to Fig. 8 for the spatial distribution.

RCMs \ Regions	BI	IP	FR	ME	SC	AL	MD	EA	FD
TSMP-MPI	25.36	17.47	19.62	25.61	29.87	24.40	19.33	17.79	22.38
CCLM-MPI	27.90	31.19	26.29	24.34	26.50	27.79	26.67	18.82	24.96
COSMO-crCLIM-MPI	18.78	31.96	25.50	18.49	27.59	33.62	24.46	16.27	23.46
REMO2009-MPI	21.81	33.04	28.35	22.39	32.63	23.50	30.18	21.92	27.22
CCLM4-CNRM	34.53	18.35	25.45	33.01	31.69	37.74	34.53	28.08	29.72
COSMO-crCLIM-CNRM	29.75	23.36	29.21	29.31	36.52	32.75	35.54	38.21	33.11
COSMO-crCLIM-NCC	34.70	23.94	30.71	23.12	39.04	30.05	33.07	23.70	29.61
REMO2015-NCC	30.16	25.39	32.05	29.06	38.37	29.72	27.54	26.69	30.20
REMO2015-IPSL	30.39	41.20	30.57	31.56	35.26	38.26	36.73	31.75	34.40
REMO2015-NOAA	30.77	25.20	21.41	16.51	37.52	24.58	32.54	19.36	26.97

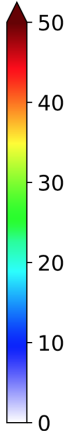


Table B2. Contribution of heat waves to the number of hot days [%], based on the data from 1976 to 2005 in the GCM-RCM multi-model ensemble, for the focus domain (FD, see Fig. 2) and the PRUDENCE regions: British Isles (BI), Iberian Peninsula (IP), France (FR), Mid-Europe (ME), Scandinavia (SC), Alps (AL), Mediterranean (MD), Eastern Europe (EA). Refer to Fig. 9 for the spatial distribution.

RCMs \ Regions	BI	IP	FR	ME	SC	AL	MD	EA	FD
TSMP-MPI	0.118	0.189	0.246	0.233	0.193	0.145	0.171	0.148	0.193
CCLM-MPI	0.246	0.305	0.468	0.395	0.175	0.326	0.318	0.319	0.301
COSMO-crCLIM-MPI	0.181	0.246	0.361	0.216	0.152	0.213	0.262	0.318	0.241
REMO2009-MPI	0.173	0.156	0.207	0.230	0.211	0.125	0.180	0.218	0.202
CCLM4-CNRM	0.185	0.199	0.356	0.244	0.290	0.121	0.125	0.218	0.233
COSMO-crCLIM-CNRM	0.111	0.187	0.236	0.157	0.309	0.106	0.143	0.293	0.232
COSMO-crCLIM-NCC	0.160	0.188	0.234	0.163	0.193	0.105	0.165	0.268	0.204
REMO2015-NCC	0.181	0.173	0.163	0.166	0.267	0.082	0.123	0.184	0.205
REMO2015-IPSL	0.287	0.112	0.219	0.214	0.203	0.112	0.084	0.108	0.174
REMO2015-NOAA	0.213	0.094	0.120	0.197	0.294	0.101	0.144	0.141	0.213




Table B3. Frequency of intense heat waves, calculated from the data between 1976 and 2005 in the GCM-RCM multi-model ensemble, for the focus domain (FD, see Fig. 2) and the PRUDENCE regions: British Isles (BI), Iberian Peninsula (IP), France (FR), Mid-Europe (ME), Scandinavia (SC), Alps (AL), Mediterranean (MD), Eastern Europe (EA). Refer to Fig. 10 for the spatial distribution.

Code and data availability. The TSMP v1.2.2 used in this work is available through <https://github.com/HPSCTerrSys/TSMP> GIT repository. The dataset from TSMP forced by MPI-ESM-LR r1i1p1 can be obtained at https://datapub.fz-juelich.de/slts/regional_climate_tsmp_hi-cam/ as open access research data.

395 *Author contributions.* The study was designed by S.K. with contributions by K.G., L.P.-S., and N.W.. L.P.-S. performed the model simulations and data processing, N.W. provided technical and programming support, C.H. provided setups, configuration, and workflow support. The analysis was developed and conducted by L.P.-S. with further inputs from S.K. and K.G.. L.P.-S. wrote the manuscript. All co-authors contributed to the interpretation of the results, active discussions, and revisions of the paper. The work was done under the supervision of S.K..

400 *Competing interests.* The authors declare that they have no conflict of interest.

Acknowledgements. This work was funded by the Helmholtz Association of German Research Centres (HGF) under the HI-CAM project (Helmholtz Initiative Climate Adaptation and Mitigation) and by the German Ministry of Education and Research (Bundesministerium für Bildung und Forschung, BMBF) under the ClimXtreme project. We are grateful to the Max-Planck Institute for performing MPI-ESM-LR r1i1p1 GCM experiment and the German Climate Computing Centre (DKRZ) for providing the MPI-ESM-LR dataset. We thank the EURO-
405 CORDEX climate modelling groups for producing and making available their model output. The authors gratefully acknowledge the Earth System Modelling Project (ESM) for funding this work by providing computing time on the ESM partition of the supercomputer JUWELS at the Jülich Supercomputing Centre (JSC) under the ESM project ID JIBG35. In addition, we thank the Centre for High-Performance Scientific Computing in Terrestrial Systems (Geoverbund ABC/J, <http://www.hp-sc-terrsys.de>) and the JSC for the computational support. Finally, we thank three anonymous reviewers for the constructive comments that helped improve this article.

410 References

- Alexander, L. V., Zhang, X., Peterson, T. C., Caesar, J., Gleason, B., Klein Tank, A. M. G., Haylock, M., Collins, D., Trewin, B., Rahimzadeh, F., Tagipour, A., Rupa Kumar, K., Revadekar, J., Griffiths, G., Vincent, L., Stephenson, D. B., Burn, J., Aguilar, E., Brunet, M., Taylor, M., New, M., Zhai, P., Rusticucci, M., and Vazquez-Aguirre, J. L.: Global observed changes in daily climate extremes of temperature and precipitation, *J. Geophys. Res. Atmos.*, 111, D05109, <https://doi.org/10.1029/2005JD006290>, 2006.
- 415 Amengual, A., Homar, V., Romero, R., Brooks, H., Ramis, C., Gordaliza, M., and Alonso, S.: Projections of heat waves with high impact on human health in Europe, *Glob. Planet. Change*, 119, 71–84, <https://doi.org/10.1016/j.gloplacha.2014.05.006>, 2014.
- Baldauf, M., Seifert, A., Förstner, J., Majewski, D., Raschendorfer, M., and Reinhardt, T.: Operational Convective-Scale Numerical Weather Prediction with the COSMO Model: Description and Sensitivities, *Mon. Weather Rev.*, 139, 3887–3905, <https://doi.org/10.1175/MWR-D-10-05013.1>, 2011.
- 420 Barlage, M., Tewari, M., Chen, F., Miguez-Macho, G., Yang, Z.-L., and Niu, G.-Y.: The effect of groundwater interaction in North American regional climate simulations with WRF/Noah-MP, *Clim. Change*, 129, 485–498, <https://doi.org/10.1007/s10584-014-1308-8>, 2015.
- Barlage, M., Chen, F., Rasmussen, R., Zhang, Z., and Miguez-Macho, G.: The Importance of Scale-Dependent Groundwater Processes in Land-Atmosphere Interactions Over the Central United States, *Geophysical Research Letters*, 48, e2020GL092171, <https://doi.org/10.1029/2020GL092171>, 2021.
- 425 Barriopedro, D., Fischer, E. M., Luterbacher, J., Trigo, R. M., and R., G.-H.: The Hot Summer of 2010: Redrawing the Temperature Record Map of Europe, *Science*, 332, 220–224, <https://doi.org/10.1126/science.1201224>, 2011.
- Barriopedro, D., García-Herrera, R., Ordóñez, C., Miralles, D. G., and Salcedo-Sanz, S.: Heat Waves: Physical Understanding and Scientific Challenges, *Rev. Geophys.*, 61, e2022RG000780, <https://doi.org/10.1029/2022RG000780>, 2023.
- Bellprat, O., Kotlarski, S., Lüthi, D., Elía, R. D., Frigon, A., Laprise, R., and Schär, C.: Objective Calibration of Regional Climate Models: Application over Europe and North America, *Journal of Climate*, 29, 819–838, <https://doi.org/10.1175/JCLI-D-15-0302.1>, 2016.
- 430 Bentsen, M., Bethke, I., Debernard, J. B., Iversen, T., Kirkevåg, A., Seland, Ø., Drange, H., Roelandt, C., Seierstad, I. A., Hoose, C., and Kristjánsson, J. E.: The Norwegian Earth System Model, NorESM1-M – Part 1: Description and basic evaluation of the physical climate, *Geosci. Model Dev.*, 6, 687–720, <https://doi.org/10.5194/gmd-6-687-2013>, 2013.
- Christensen, J. H. and Christensen, O. B.: A summary of the PRUDENCE model projections of changes in European climate by the end of this century, *Clim. Change*, 81, 7–30, <https://doi.org/10.1007/s10584-006-9210-7>, 2007.
- 435 Christensen, O. B. and Kjellström, E.: Partitioning uncertainty components of mean climate and climate change in a large ensemble of European regional climate model projections, *Clim. Dyn.*, 54, 4293–4308, <https://doi.org/10.1007/s00382-020-05229-y>, 2020.
- Christidis, N., Jones, G., and Stott, P.: Dramatically increasing chance of extremely hot summers since the 2003 European heatwave, *Nature Clim. Change*, 5, 46–50, <https://doi.org/10.1038/nclimate2468>, 2015.
- 440 Cornes, R. C., van der Schrier, G., van den Besselaar, E. J. M., and Jones, P. D.: An Ensemble Version of the E-OBS Temperature and Precipitation Data Sets, *J. Geophys. Res. Atmos.*, 123, 9391–9409, <https://doi.org/10.1029/2017JD028200>, 2018.
- Daac, L.: Global 30 arc-second elevation data set GTOPO30, Land process distributed active archive center, 20, <https://www.usgs.gov/centers/eros/science/usgs-eros-archive-digital-elevation-global-30-arc-second-elevation-gtopo30>, 2004.
- 445 Dee, D. P., Uppala, S. M., Simmons, A. J., Berrisford, P., Poli, P., Kobayashi, S., Andrae, U., Balmaseda, M. A., Balsamo, G., Bauer, P., Bechtold, P., Beljaars, A. C. M., van de Berg, L., Bidlot, J., Bormann, N., Delsol, C., Dragani, R., Fuentes, M., Geer, A. J., Haimberger, L., Healy, S. B., Hersbach, H., Hólm, E. V., Isaksen, L., Kallberg, P., Koehler, M., Matricardi, M., McNally, A. P., Monge-Sanz, B. M., Mor-

- crette, J.-J., Park, B.-K., Peubey, C., de Rosnay, P., Tavolato, C., Thépaut, J.-N., and Vitart, F.: The ERA-Interim reanalysis: configuration and performance of the data assimilation system, *Q. J. R. Meteorol. Soc.*, 137, 553–597, <https://doi.org/10.1002/qj.828>, 2011.
- 450 Déqué, M., Rowell, D. P., Lüthi, D., Giorgi, F., Christensen, J. H., Rockel, B., Jacob, D., Kjellström, E., de Castro, M., and van den Hurk, B.: An intercomparison of regional climate simulations for Europe: assessing uncertainties in model projections, *Clim. Change*, 81, 53–70, <https://doi.org/10.1007/s10584-006-9228-x>, 2007.
- Déqué, M., Somot, S., Sanchez-Gomez, E., Goodess, C. M., Jacob, D., Lenderink, G., and Christensen, O. B.: The spread amongst ENSEMBLES regional scenarios: regional climate models, driving general circulation models and interannual variability, *Clim. Change*, 38, 951–964, <https://doi.org/10.1007/s00382-011-1053-x>, 2012.
- 455 Dirmeyer, P. A., Balsamo, G., Blyth, E. M., Morrison, R., and Cooper, H. M.: Land-Atmosphere Interactions Exacerbated the Drought and Heatwave Over Northern Europe During Summer 2018, *AGU Advances*, 2, e2020AV000283, <https://doi.org/10.1029/2020AV000283>, 2021.
- Dufresne, J.-L., Foujols, M.-A., Denvil, S., and et al.: Climate change projections using the IPSL-CM5 Earth System Model: from CMIP3 to CMIP5, *Clim. Dyn.*, 40, 2123–2165, <https://doi.org/10.1007/s00382-012-1636-1>, 2013.
- 460 Dunne, J. P., John, J. G., Adcroft, A. J., Griffies, S. M., Hallberg, R. W., Shevliakova, E., Stouffer, R. J., Cooke, W., Dunne, K. A., Harrison, M. J., Krasting, J. P., Malyshev, S. L., Milly, P. C. D., Philipps, P. J., Sentman, L. T., Samuels, B. L., Spelman, M. J., Winton, M., Wittenberg, A. T., and Zadeh, N.: GFDL’s ESM2 Global Coupled Climate–Carbon Earth System Models. Part I: Physical Formulation and Baseline Simulation Characteristics, *J. Clim.*, 25, 6646–6665, <https://doi.org/10.1175/JCLI-D-11-00560.1>, 2012.
- Duscher, K., Günther, A., Richts, A., Clos, P., Philipp, U., and Struckmeier, W.: The GIS layers of the “International Hydrogeological Map of Europe 1:1,500,000” in a vector format, *Hydrogeol. J.*, 23, 1867–1875, <https://doi.org/10.1007/s10040-015-1296-4>, 2015.
- 465 Erdenebat, E. and Tomonori, S.: Role of soil moisture-atmosphere feedback during high temperature events in 2002 over Northeast Eurasia, *Prog. Earth. Planet. Sci.*, 5, 37, <https://doi.org/10.1186/s40645-018-0195-4>, 2018.
- Evin, G., Somot, S., and Hingray, B.: Balanced estimate and uncertainty assessment of European climate change using the large EURO-CORDEX regional climate model ensemble, *Earth Syst. Dyn.*, 12, 1543–1569, <https://doi.org/10.5194/esd-12-1543-2021>, 2021.
- 470 FAO: FAO/UNESCO Soil Map of the World, Revised Legend, with corrections and updates, World Soil Resources Report 60, FAO, Rome, <https://www.fao.org/3/bl892e/bl892e.pdf>, 1988.
- Fernández, J., Frías, M. D., Cabos, W. D., Cofiño, A. S., Domínguez, M., Fita, L., Gaertner, M. A., García-Díez, M., Gutiérrez, J. M., Jiménez-Guerrero, P., Liguori, G., Montávez, J. P., Romera, R., and Sánchez, E.: Consistency of climate change projections from multiple global and regional model intercomparison projects, *Clim. Dyn.*, 52, 1139–1156, <https://doi.org/10.1007/s00382-018-4181-8>, 2019.
- 475 Fischer, E. M. and Schär, C.: Consistent geographical patterns of changes in high-impact European heatwaves, *Nat. Geosci.*, 3, 398–403, <https://doi.org/10.1038/ngeo866>, 2010.
- Fischer, E. M., Seneviratne, S. I., Lüthi, D., and Schär, C.: Contribution of land-atmosphere coupling to recent European summer heat waves, *Geophys. Res. Lett.*, 34, L06707, <https://doi.org/10.1029/2006GL029068>, 2007.
- Frich, P., Alexander, L. V., Della-Marta, P., Gleason, B., Haylock, M., Klein Tank, A. M. G., and Peterson, T.: Observed coherent changes in climatic extremes during the second half of the twentieth century, *Clim. Res.*, 19, 193–212, <https://doi.org/10.3354/cr019193>, 2002.
- 480 Friedl, M., McIver, D., Hodges, J., Zhang, X., Muchoney, D., Strahler, A., Woodcock, C., Gopal, S., Schneider, A., Cooper, A., Baccini, A., Gao, F., and Schaaf, C.: Global land cover mapping from MODIS: algorithms and early results, *Remote Sens. Environ.*, 83, 287–302, [https://doi.org/10.1016/S0034-4257\(02\)00078-0](https://doi.org/10.1016/S0034-4257(02)00078-0), 2002.

- 485 Furusho-Percot, C., Goergen, K., Hartick, C., Kulkarni, K., Keune, J., and Kollet, S.: Pan-European groundwater to atmosphere terrestrial systems climatology from a physically consistent simulation, *Sci. Data*, 6, 320, <https://doi.org/10.1038/s41597-019-0328-7>, 2019.
- Furusho-Percot, C., Goergen, K., Hartick, C., Poshyvailo-Strube, L., and Kollet, S.: Groundwater Model Impacts Multiannual Simulations of Heat Waves, *Geophys. Res. Lett.*, 49, e2021GL096781, <https://doi.org/10.1029/2021GL096781>, 2022.
- 490 Gasper, F., Goergen, K., Shrestha, P., Sulis, M., Rihani, J., Geimer, M., and Kollet, S.: Implementation and scaling of the fully coupled Terrestrial Systems Modeling Platform (TerrSysMP v1.0) in a massively parallel supercomputing environment – a case study on JUQUEEN (IBM Blue Gene/Q), *Geosci. Model Dev.*, 7, 2531–2543, <https://doi.org/10.5194/gmd-7-2531-2014>, 2014.
- Giorgetta, M. A., Jungclaus, J., Reick, C. H., Legutke, S., Bader, J., Böttinger, M., Brovkin, V., Crueger, T., Esch, M., Fieg, K., Glushak, K., Gayler, V., Haak, H., Hollweg, H.-D., Ilyina, T., Kinne, S., Kornblueh, L., Matei, D., Mauritsen, T., Mikolajewicz, U., Mueller, W., Notz, D., Pithan, F., Raddatz, T., Rast, S., Redler, R., Roeckner, E., Schmidt, H., Schnur, R., Segschneider, J., Six, K. D., Stockhause, M., Timmreck, C., Wegner, J., Widmann, H., Wieners, K.-H., Claussen, M., Marotzke, J., and Stevens, B.: Climate and carbon cycle changes from 1850 to 2100 in MPI-ESM simulations for the Coupled Model Intercomparison Project phase 5, *J. Adv. Model. Earth Syst.*, 495 5, 572–597, <https://doi.org/10.1002/jame.20038>, 2013.
- Giorgi, F. and Gutowski, W. J.: Regional Dynamical Downscaling and the CORDEX Initiative, *Annu. Rev. Environ. Resour.*, 40, 467–490, <https://doi.org/10.1146/annurev-environ-102014-021217>, 2015.
- Gleeson, T., Moosdorf, N., Hartmann, J., and van Beek, L. P. H.: A glimpse beneath earth’s surface: GLobal HYdrogeology MaPS (GL-HYMPS) of permeability and porosity, *Geophys. Res. Lett.*, 41, 3891–3898, <https://doi.org/10.1002/2014GL059856>, 2014.
- 500 Grasselt, René and Schüttemeyer, D., Warrach-Sagi, K., Ament, F., and Simmer, C.: Validation of TERRA-ML with discharge measurements, *Meteorol. Z.*, 17, 763–773, <https://doi.org/10.1127/0941-2948/2008/0334>, 2008.
- Gutowski, W. J., Giorgi, F., Timbal, B., Frigon, A., Jacob, D., Kang, H.-S., Raghavan, K., Lee, B., Lennard, C., Nikulin, G., O’Rourke, E., Rixen, M., Solman, S., Stephenson, T., and Tangang, F.: WCRP COordinated Regional Downscaling EXperiment (CORDEX): a diagnostic MIP for CMIP6, *Geosci. Model Dev.*, 9, 4087–4095, <https://doi.org/10.5194/gmd-9-4087-2016>, 2016.
- 505 Haghighi, E., Short Gianotti, D. J., Akbar, R., Salvucci, G. D., and Entekhabi, D.: Soil and Atmospheric Controls on the Land Surface Energy Balance: A Generalized Framework for Distinguishing Moisture-Limited and Energy-Limited Evaporation Regimes, *Water Resour. Res.*, 54, 1831–1851, <https://doi.org/https://doi.org/10.1002/2017WR021729>, 2018.
- Hari, V., Rakovec, O., Markonis, Y., Hanel, M., and Kumar, R.: Increased future occurrences of the exceptional 2018-2019 Central European drought under global warming, *Sci. Rep.*, 10, 12207, <https://doi.org/10.1038/s41598-020-68872-9>, 2020.
- 510 Hartick, C., Furusho-Percot, C., Goergen, K., and Kollet, S.: An Interannual Probabilistic Assessment of Subsurface Water Storage Over Europe Using a Fully Coupled Terrestrial Model, *Water Resour. Res.*, 57, e2020WR027828, <https://doi.org/https://doi.org/10.1029/2020WR027828>, 2021.
- Hartick, C., Furusho-Percot, C., Clark, M. P., and Kollet, S.: An Interannual Drought Feedback Loop Affects the Surface Energy Balance and Cloud Properties, *Geophys. Res. Lett.*, 49, e2022GL100924, <https://doi.org/10.1029/2022GL100924>, 2022.
- 515 Hawkins, E. and Sutton, R.: The Potential to Narrow Uncertainty in Regional Climate Predictions, *Bull. Am. Meteorol. Soc.*, 90, 1095–1108, <https://doi.org/10.1175/2009BAMS2607.1>, 2009.
- Horton, R. M., Mankin, J. S., Lesk, C., Coffel, E., and Raymond, C.: Review of Recent Advances in Research on Extreme Heat Events, *Curr. Clim. Change. Rep.*, 2, 242–259, <https://doi.org/10.1007/s40641-016-0042-x>, 2016.

- 520 Iles, C. E., Vautard, R., Strachan, J., Joussaume, S., Eggen, B. R., and Hewitt, C. D.: The benefits of increasing resolution in global and regional climate simulations for European climate extremes, *Geosci. Model Dev.*, 13, 5583–5607, <https://doi.org/10.5194/gmd-13-5583-2020>, 2020.
- Jach, L., Schwitalla, T., Branch, O., Warrach-Sagi, K., and Wulfmeyer, V.: Sensitivity of land–atmosphere coupling strength to changing atmospheric temperature and moisture over Europe, *Earth Syst. Dynam.*, 13, 109–132, <https://doi.org/10.5194/esd-13-109-2022>, 2022.
- 525 Jacob, D. and Podzun, R.: Sensitivity studies with the regional climate model REMO, *Meteorol. Atmos. Phys.*, 63, 119–129, <https://doi.org/10.1007/BF01025368>, 1997.
- Jacob, D., Teichmann, C., Sobolowski, S., and et al.: Regional climate downscaling over Europe: perspectives from the EURO-CORDEX community, *Reg. Environ. Change*, 20, 51, <https://doi.org/10.1007/s10113-020-01606-9>, 2020.
- Kautz, L.-A., Martius, O., Pfahl, S., Pinto, J. G., Ramos, A. M., Sousa, P. M., and Woollings, T.: Atmospheric blocking and weather extremes over the Euro-Atlantic sector – a review, *Weather Clim. Dynam.*, 3, 305–336, <https://doi.org/10.5194/wcd-3-305-2022>, 2022.
- 530 Keune, J., Gasper, F., Goergen, K., Hense, A., Shrestha, P., Sulis, M., and Kollet, S.: Studying the influence of groundwater representations on land surface–atmosphere feedbacks during the European heat wave in 2003, *J. Geophys. Res. Atmos.*, 121, 13 301–13 325, <https://doi.org/10.1002/2016JD025426>, 2016.
- Kollet, S. J. and Maxwell, R. M.: Integrated surface–groundwater flow modeling: A free-surface overland flow boundary condition in a parallel groundwater flow model, *Adv. Water. Resour.*, 29, 945–958, <https://doi.org/10.1016/j.advwatres.2005.08.006>, 2006.
- 535 Kollet, S. J. and Maxwell, R. M.: Capturing the influence of groundwater dynamics on land surface processes using an integrated, distributed watershed model, *Water Resour. Res.*, 44, W02402, <https://doi.org/10.1029/2007WR006004>, 2008.
- Kuffour, B. N. O., Engdahl, N. B., Woodward, C. S., Condon, L. E., Kollet, S., and Maxwell, R. M.: Simulating coupled surface–subsurface flows with ParFlow v3.5.0: capabilities, applications, and ongoing development of an open-source, massively parallel, integrated hydro-logic model, *Geosci. Model Dev.*, 13, 1373–1397, <https://doi.org/10.5194/gmd-13-1373-2020>, 2020.
- 540 Landerer, F. W., Flechtner, F. M., Save, H., Webb, F. H., Bandikova, T., Bertiger, W. I., Bettadpur, S. V., Byun, S. H., Dahle, C., Dobslaw, H., Fahnestock, E., Harvey, N., Kang, Z., Kruizinga, G. L. H., Loomis, B. D., McCullough, C., Murböck, M., Nagel, P., Paik, M., Pie, N., Poole, S., Strelakov, D., Tamisiea, M. E., Wang, F., Watkins, M. M., Wen, H.-Y., Wiese, D. N., and Yuan, D.-N.: Extending the Global Mass Change Data Record: GRACE Follow-On Instrument and Science Data Performance, *Geophys. Res. Lett.*, 47, e2020GL088 306, <https://doi.org/10.1029/2020GL088306>, 2020.
- 545 Lhotka, O. and Kyselý, J.: Characterizing joint effects of spatial extent, temperature magnitude and duration of heat waves and cold spells over Central Europe, *Int. J. Climatol.*, 35, 1232–1244, <https://doi.org/10.1002/joc.4050>, 2015.
- Lhotka, O., Kyselý, J., and Plavcová, E.: Evaluation of major heat waves’ mechanisms in EURO-CORDEX RCMs over Central Europe, *Clim. Dyn.*, 50, 4249–4262, <https://doi.org/10.1007/s00382-017-3873-9>, 2018.
- 550 Liang, X., Xie, Z., and Huang, M.: A new parameterization for surface and groundwater interactions and its impact on water budgets with the variable infiltration capacity (VIC) land surface model, *J. Geophys. Res.*, 108, 8613, <https://doi.org/https://doi.org/10.1029/2002JD003090>, 2003.
- Liu, X., He, B., Guo, L., Huang, L., and Chen, D.: Similarities and Differences in the Mechanisms Causing the European Summer Heatwaves in 2003, 2010, and 2018, *Earth’s Future*, 8, e2019EF001386, <https://doi.org/10.1029/2019EF001386>, 2020.
- 555 Ma, Y., Montzka, C., Naz, B. S., and Kollet, S.: Advancing AI-based pan-European groundwater monitoring, *Environ. Res. Lett.*, 17, 114 037, <https://doi.org/10.1088/1748-9326/ac9c1e>, 2022.

- Martínez-de la Torre, A. and Miguez-Macho, G.: Groundwater influence on soil moisture memory and land–atmosphere fluxes in the Iberian Peninsula, *Hydrol. Earth Syst. Sci.*, 23, 4909–4932, <https://doi.org/10.5194/hess-23-4909-2019>, 2019.
- 560 Masson-Delmotte, V., Zhai, P., Pirani, A., Connors, S., Péan, C., Berger, S., Caud, N. and Chen, Y., Goldfarb, L., Gomis, M., Huang, M., Leitzell, K., Lonnoy, I., Matthews, J., Maycock, T., Waterfield, T., Yelekçi, O., Yu, R., and B., Z., eds.: IPCC report, *Climate Change 2021: The Physical Science Basis. Contribution of Working Group I to the Sixth Assessment Report of the Intergovernmental Panel on Climate Change*, Cambridge University Press, Cambridge, United Kingdom and New York, NY, USA, https://www.ipcc.ch/report/ar6/wg1/downloads/report/IPCC_AR6_WGI_FullReport.pdf, 2021.
- 565 Maxwell, R. M. and Condon, L. E.: Connections between groundwater flow and transpiration partitioning, *Science*, 353, 377–380, <https://doi.org/10.1126/science.aaf7891>, 2016.
- Maxwell, R. M. and Miller, N. L.: Development of a Coupled Land Surface and Groundwater Model, *J. Hydrometeorol.*, 6, 233–247, <https://doi.org/10.1175/JHM422.1>, 2005.
- Maxwell, R. M., Chow, F. K., and Kollet, S. J.: The groundwater–land–surface–atmosphere connection: Soil moisture effects on the atmospheric boundary layer in fully-coupled simulations, *Adv. Water Resour.*, 30, 2447–2466, <https://doi.org/10.1016/j.advwatres.2007.05.018>, 570 2007.
- Mearns, L. O., Lettenmaier, D. P., and McGinnis, S.: Uses of Results of Regional Climate Model Experiments for Impacts and Adaptation Studies: the Example of NARCCAP, *Curr. Clim. Change Rep.*, 1, 1–9, <https://doi.org/10.1007/s40641-015-0004-8>, 2015.
- Molina, M. O., Sánchez, E., and Gutiérrez, C.: Future heat waves over the Mediterranean from an Euro-CORDEX regional climate model ensemble, *Sci. Rep.*, 10, 8801, <https://doi.org/10.1038/s41598-020-65663-0>, 2020.
- 575 Mu, M., Pitman, A. J., De Kauwe, M. G., Ukkola, A. M., and Ge, J.: How do groundwater dynamics influence heatwaves in southeast Australia?, *Weather Clim. Extrem.*, 37, 100479, <https://doi.org/10.1016/j.wace.2022.100479>, 2022.
- Nairn, J. R. and Fawcett, R. J. B.: The excess heat factor: a metric for heatwave intensity and its use in classifying heatwave severity, *Int. J. Environ. Res. Public Health*, 12, 227–253, <https://doi.org/10.3390/ijerph120100227>, 2014.
- Naz, B. S., Sharples, W., Ma, Y., Goergen, K., and Kollet, S.: Continental-scale evaluation of a fully distributed coupled land surface and groundwater model, ParFlow-CLM (v3.6.0), over Europe, *Geosci. Model Dev.*, 16, 1617–1639, <https://doi.org/10.5194/gmd-16-1617-2023>, 580 2023.
- Niu, G.-Y., Yang, Z.-L., Dickinson, R. E., Gulden, L. E., and Su, H.: Development of a simple groundwater model for use in climate models and evaluation with Gravity Recovery and Climate Experiment data, *J. Geophys. Res. Atmos.*, 112, D07103, <https://doi.org/10.1029/2006JD007522>, 2007.
- 585 Oleson, K., Dai, Y., Bonan, G. B., Bosilovich, M., Dickinson, R., Dirmeyer, P., and et al.: Technical Description of the Community Land Model (CLM) (No. NCAR/TN-461+STR), Tech. rep., University Corporation for Atmospheric Research, <https://doi.org/10.5065/D6N877R0>, 2004.
- Oleson, K. W., Niu, G.-Y., Yang, Z.-L., Lawrence, D. M., Thornton, P. E., Lawrence, P. J., Stöckli, R., Dickinson, R. E., Bonan, G. B., Levis, S., Dai, A., and Qian, T.: Improvements to the Community Land Model and their impact on the hydrological cycle, *J. Geophys. Res. Biogeosci.*, 113, G01021, <https://doi.org/10.1029/2007JG000563>, 590 2008.
- Pal, J. S. and Eltahir, E. A. B.: Pathways Relating Soil Moisture Conditions to Future Summer Rainfall within a Model of the Land–Atmosphere System, *J. Climate*, 14, 1227–1242, [https://doi.org/https://doi.org/10.1175/1520-0442\(2001\)014<1227:PRSMCT>2.0.CO;2](https://doi.org/https://doi.org/10.1175/1520-0442(2001)014<1227:PRSMCT>2.0.CO;2), 2001.

- Perkins, S. E. and Alexander, L. V.: On the Measurement of Heat Waves, *J. Clim.*, 26, 4500–4517, <https://doi.org/10.1175/JCLI-D-12-00383.1>, 2013.
- Plavcová, E. and Kyselý, J.: Overly persistent circulation in climate models contributes to overestimated frequency and duration of heat waves and cold spells, *Clim. Dyn.*, 46, 2805–2820, <https://doi.org/10.1007/s00382-015-2733-8>, 2016.
- Pothapakula, P. K., Primo, C., Sørland, S., and Ahrens, B.: The synergistic impact of ENSO and IOD on Indian summer monsoon rainfall in observations and climate simulations – an information theory perspective, *Earth Syst. Dynam.*, 11, 903–923, <https://doi.org/10.5194/esd-11-903-2020>, 2020.
- Prein, A. F., Gobiet, A., Truhetz, H., Keuler, K., Goergen, K., Teichmann, C., Fox Maule, C., van Meijgaard, E., Déqué, M., Nikulin, G., Vautard, R., Colette, A., Kjellström, E., and Jacob, D.: Precipitation in the EURO-CORDEX 0.11° and 0.44° simulations: high resolution, high benefits?, *Clim. Dyn.*, 46, 383–412, <https://doi.org/10.1007/s00382-015-2589-y>, 2016.
- Rockel, B., Will, A., and Hense, A.: The Regional Climate Model COSMO-CLM (CCLM), *Meteorol. Z.*, 17, 347–348, <https://doi.org/10.1127/0941-2948/2008/0309>, 2008.
- Rummukainen, M.: Added value in regional climate modeling, *WIREs Clim. Change*, 7, 145–159, <https://doi.org/10.1002/wcc.378>, 2016.
- Russo, S., Sillmann, J., and Fischer, E. M.: Top ten European heatwaves since 1950 and their occurrence in the coming decades, *Environ. Res. Lett.*, 10, 124003, <https://doi.org/10.1088/1748-9326/10/12/124003>, 2015.
- Schlemmer, L., Schär, C., Lüthi, D., and Strebel, L.: A Groundwater and Runoff Formulation for Weather and Climate Models, *J. Adv. Model. Earth Syst.*, 10, 1809–1832, <https://doi.org/10.1029/2017MS001260>, 2018.
- Seneviratne, S. I., Lüthi, D., Litschi, M., and Schär, C.: Land–atmosphere coupling and climate change in Europe, *Nature*, 443, 205–209, <https://doi.org/10.1038/nature05095>, 2006.
- Seneviratne, S. I., Corti, T., Davin, E. L., Hirschi, M., Jaeger, E. B., Lehner, I., Orlowsky, B., and Teuling, A. J.: Investigating soil moisture–climate interactions in a changing climate: A review, *Earth-Sci. Rev.*, 99, 125–161, <https://doi.org/10.1016/j.earscirev.2010.02.004>, 2010.
- Shrestha, P., Sulis, M., Masbou, M., Kollet, S., and Simmer, C.: A Scale-Consistent Terrestrial Systems Modeling Platform Based on COSMO, CLM, and ParFlow, *Mon. Weather Rev.*, 142, 3466–3483, <https://doi.org/10.1175/MWR-D-14-00029.1>, 2014.
- Song, Y. M., Wang, Z. F., Qi, L. L., and Huang, A. N.: Soil Moisture Memory and Its Effect on the Surface Water and Heat Fluxes on Seasonal and Interannual Time Scales, *J. Geophys. Res. Atmos.*, 124, 10 730–10 741, <https://doi.org/10.1029/2019JD030893>, 2019.
- Sørland, S. L., Schär, C., Lüthi, D., and Kjellström, E.: Bias patterns and climate change signals in GCM-RCM model chains, *Environ. Res. Lett.*, 13, 074017, <https://doi.org/10.1088/1748-9326/aacc77>, 2018.
- Stegehuis, A. I., Vogel, M. M., Vautard, R., Ciais, P., Teuling, A. J., and Seneviratne, S. I.: Early Summer Soil Moisture Contribution to Western European Summer Warming, *J. Geophys. Res. Atmos.*, 126, e2021JD034646, <https://doi.org/10.1029/2021JD034646>, 2021.
- Stott, P. A., Stone, D. A., and Allen, M. R.: Human contribution to the European heatwave of 2003, *Nature*, 432, 610–614, <https://doi.org/10.1038/nature03089>, 2004.
- Sulikowska, A. and Wypych, A.: Summer temperature extremes in Europe: how does the definition affect the results?, *Theor. Appl. Climatol.*, 141, 19–30, <https://doi.org/10.1007/s00704-020-03166-8>, 2020.
- Taylor, K. E., Stouffer, R. J., and Meehl, G. A.: An Overview of CMIP5 and the Experiment Design, *Bull. Am. Meteorol. Soc.*, 93, 485–498, <https://doi.org/10.1175/BAMS-D-11-00094.1>, 2012.
- Teuling, A. J., Uijlenhoet, R., van den Hurk, B., and Seneviratne, S. I.: Parameter Sensitivity in LSMs: An Analysis Using Stochastic Soil Moisture Models and ELDAS Soil Parameters, *J. Hydrometeorol.*, 10, 751–765, <https://doi.org/10.1175/2008JHM1033.1>, 2009.

- Tomczyk, A. M. and Bednorz, E.: Heat waves in Central Europe and their circulation conditions, *Int. J. Climatol.*, 36, 770–782, <https://doi.org/10.1002/joc.4381>, 2016.
- Torma, C., Giorgi, F., and Coppola, E.: Added value of regional climate modeling over areas characterized by complex terrain—Precipitation over the Alps, *J. Geophys. Res. Atmos.*, 120, 3957–3972, <https://doi.org/https://doi.org/10.1002/2014JD022781>, 2015.
- 635
- Turco, M., Sanna, A., Herrera, S., Llasat, M.-C., and Gutiérrez, J. M.: Large biases and inconsistent climate change signals in ENSEMBLES regional projections, *Clim. Change*, 120, 859–869, <https://doi.org/10.1007/s10584-013-0844-y>, 2013.
- Valecke, S.: The OASIS3 coupler: a European climate modelling community software, *Geosci. Model Dev.*, 6, 373–388, <https://doi.org/10.5194/gmd-6-373-2013>, 2013.
- 640
- Vautard, R., Gobiet, A., Jacob, D., and et al.: The simulation of European heat waves from an ensemble of regional climate models within the EURO-CORDEX project, *Clim. Dyn.*, 41, 2555–2575, <https://doi.org/10.1007/s00382-013-1714-z>, 2013.
- Vogel, M. M., Zscheischler, J., and Seneviratne, S. I.: Varying soil moisture–atmosphere feedbacks explain divergent temperature extremes and precipitation projections in central Europe, *Earth Syst. Dyn.*, 9, 1107–1125, <https://doi.org/10.5194/esd-9-1107-2018>, 2018.
- Vogt, J., Soille, P., De Jager, A., Rimaviciute, E., Mehl, W., Foisneau, S., Bodis, K., Dusart, J., Paracchini, M., Haastrup, P., and Bamps, C.: A pan-European River and Catchment Database, JRC Reference Report, Joint Research Centre, Institute for Environment and Sustainability, <https://doi.org/10.2788/35907>, 2007.
- 645
- Volodre, A., Sanchez-Gomez, E., Salas y Méliá, D., and et al: The CNRM-CM5.1 global climate model: description and basic evaluation, *Clim. Dyn.*, 40, 2091–2121, <https://doi.org/10.1007/s00382-011-1259-y>, 2013.
- Yang, L., Sun, G., Zhi, L., and Zhao, J.: Negative soil moisture-precipitation feedback in dry and wet regions, *Sci Rep*, 8, 4026, <https://doi.org/10.1038/s41598-018-22394-7>, 2018.
- 650
- Yin, C., Yang, Y., Chen, X., Yue, X., Liu, Y., and Xin, Y.: Changes in global heat waves and its socioeconomic exposure in a warmer future, *Clim. Risk Manag.*, 38, 100 459, <https://doi.org/10.1016/j.crm.2022.100459>, 2022.
- Yule, E. L., Hegerl, G., Schurer, A., and Hawkins, E.: Using early extremes to place the 2022 UK heat waves into historical context, *Atmos. Sci. Lett.*, e1159, <https://doi.org/10.1002/asl.1159>, 2023.
- 655
- Zhang, R., Sun, C., Zhu, J., Zhang, R., and Li, W.: Increased European heat waves in recent decades in response to shrinking Arctic sea ice and Eurasian snow cover, *npj Clim. Atmos. Sci.*, 3, 7, <https://doi.org/10.1038/s41612-020-0110-8>, 2020.
- Zhang, X., Hegerl, G., Zwiers, F., and Kenyon, J.: Avoiding Inhomogeneity in Percentile-Based Indices of Temperature Extremes, *J. Clim.*, 38, 1641–1651, <https://doi.org/10.1175/JCLI3366.1>, 2005.
- Zhang, X., Alexander, L., Hegerl, G. C., Jones, P., Tank, A. K., Peterson, T. C., Trewin, B., and Zwiers, F. W.: Indices for monitoring changes in extremes based on daily temperature and precipitation data, *WIRES Clim. Change*, 2, 851–870, <https://doi.org/10.1002/wcc.147>, 2011.
- 660